SMALL- AND WAITING-TIME BEHAVIOUR OF THE THIN-FILM EQUATION.

READING UNIVERSITY NUMERICAL ANALYSIS REPORT 9/06

JAMES F. BLOWEY[*][§], JOHN R. KING[†], AND STEPHEN LANGDON[‡][§][¶]

Abstract. We consider the small-time behaviour of interfaces of zero contact angle solutions to the thin-film equation. For a certain class of initial data, through asymptotic analyses, we deduce a wide variety of behaviour for the free boundary point. These are supported by extensive numerical simulations.

Key words. thin-film, waiting-time, interface, nonlinear degenerate parabolic

AMS subject classifications. 35R35, 35K35, 35K55, 35K65, 65M60

1. Introduction. This paper is concerned with the small-time behaviour of interfaces of zero contact angle solutions to the "thin-film" equation

$$\frac{\partial h}{\partial t} = -\frac{\partial}{\partial x}\left(h^n \frac{\partial^3 h}{\partial x^3}\right), \tag{1.1a}$$

$$\text{with} \quad h = h_0(x) \quad \text{at } t = 0 \quad \text{and} \tag{1.1b}$$

$$h = \frac{\partial h}{\partial x} = h^n \frac{\partial^3 h}{\partial x^3} = 0 \quad \text{at } x = s(t), \tag{1.1c}$$

where $h \geq 0$ represents the thickness of a fluid film and $x = s(t)$ denotes the right-hand interface (with $h \equiv 0$ for $x > s(t)$); since we are concerned with the local behaviour at such an interface we need not specify conditions at any left-hand moving boundary. The first boundary condition of (1.1c) defines the moving boundary (as the point at which the film thickness reaches zero), the second ensures a zero contact angle, and the third represents conservation of mass.

In the last few years the range $0 < n \leq 3$ has been considered in the literature from a modelling point of view. With $n = 3$, (1.1a–c) models the lubrication approximation of a surface tension driven thin viscous film spreading on a solid horizontal surface, with a no-slip condition at the solid/liquid/air interface [5, 6, 10, 11, 12, 14, 30]. However, the no-slip condition implies an infinite force at the interface [18, 24]. To avoid this, more realistic models allowing slip have been proposed (see e.g. [4, 19, 23]) for which it has been shown that the qualitative behaviour of solutions in the vicinity of the interface corresponds to that of the solution of (1.1a–c) with $n \in (0, 3)$; this applies to questions of spreading or non-spreading as well as to questions of locally preserved positivity and local film rupture [16]. With $n \in (0, 3)$ it is also well known (see e.g. [7, 8]) that (1.1a–c) admits solutions with a finite speed of propagation property, i.e. $s(t)$ represents a moving boundary, which moves at finite speed.

In this paper we thus consider only values of n in the moving front regime $0 < n < 3$, and we assume further that the film is thick enough that Van der Waals forces

[*]Department of Mathematical Sciences, University of Durham, DH1 3LE, U.K. (`j.f.blowey@durham.ac.uk`).

[†]School of Mathematical Sciences, University of Nottingham, University Park, Nottingham, NG7 2RD, U.K. (`John.King@nottingham.ac.uk`).

[‡]Department of Mathematics, University of Reading, Whiteknights, PO Box 220, Berkshire RG6 6AX, U.K. (`s.langdon@reading.ac.uk`).

play no part. When considering solutions to (1.1a–c), the primary physical question is often to do with the movement of the free boundary. Where $h = 0$ there is no diffusion in (1.1a), and this can lead to waiting-time behaviour, where the interface remains stationary for a period before moving; alternatively the interface may either advance or retreat immediately. A determination of the regimes in which such behaviour can occur has considerable implications regarding the possibility of film rupture in the presence of a very thin pre-wetting layer; see e.g. [27].

There has been much recent effort in the literature to answer outstanding questions about the initial movement of the interface. Theoretical results in [4, 5] have shown that the interface cannot retreat if $n \geq 3/2$, but that film rupture may occur for $n < 1/2$ (see also [13, 14]). Moreover, numerical evidence [4, 10, 12] suggests that for small values of n solutions which are initially strictly positive may vanish at some point x_0 after a finite time t_0, with the solution becoming zero on a set of positive measure shortly after the finite time singularity, a phenomenon called "dead core" in other fields. The existence of a *critical exponent* (a value of $n_* > 0$ for which solutions stay positive for $n > n_*$ and where finite-time singularities are possible for $n \leq n_*$) has been conjectured in [11], where it is remarked that numerical simulations suggest $1 < n_* < 3.5$. Our results below support and clarify these conjectures; in particular, here we provide the first concrete solutions to (1.1a–c) displaying retreat.

As explained in [27], subsequent to any waiting time the local behaviour of solutions to (1.1a–c) takes the form

$$h \sim \left(\frac{n^3 \dot{s}}{3(3-n)(2n-3)} (s-x)^3 \right)^{\frac{1}{n}} \quad \text{as } x \to s^-, \quad \text{for } \tfrac{3}{2} < n < 3, \qquad (1.2)$$

$$h \sim \left(\frac{3}{4} \dot{s}(s-x)^3 \ln\left[1/(s-x)\right] \right)^{\frac{2}{3}} \quad \text{as } x \to s^-, \quad \text{for } n = \tfrac{3}{2}, \qquad (1.3)$$

$$h \sim B(t)(s-x)^2 \quad \text{as } x \to s^-, \quad \text{for } n < \tfrac{3}{2}. \qquad (1.4)$$

With $0 < n < 3$, in (1.2) we require that $\dot{s} > 0$, whereas in (1.4) the interface velocity $\dot{s}$ may take either sign, with $B(t)$ determined as part of the solution. One of the key motivations for the current analysis is to provide criteria under which $\dot{s} < 0$ holds for sufficiently small time; since $\dot{s} > 0$ typically holds for large times, for example for the Cauchy problem with initial data of finite mass, a large-time analysis provides no insight into such matters.

For definiteness, we shall consider the case

$$h_0(x) \sim A_0(x_0 - x)^\alpha + C_0(x_0 - x)^\beta \quad \text{as } x \to x_0^- \qquad (1.5)$$

where A_0, α and β are positive constants with $\beta > \alpha$, C_0 is a constant and $x_0 = s(0)$.

Extensive studies of the small-time behaviour have already been done for the corresponding second-order problem, the porous-medium equation.

$$\frac{\partial h}{\partial t} = \frac{\partial}{\partial x}\left(h^n \frac{\partial h}{\partial x} \right) \qquad (1.6)$$

with $n > 0$. We present our results in this context. The variety of possible small-time behaviours for (1.1a–c) is summarised in Figure 1.1, and can be characterised as follows;

(i) For α greater than some critical value, the interface "waits" for some finite time t_w, whereby

$$s(t) = x_0 \quad \text{for } 0 \leq t \leq t_w,$$

after which time it moves (see also [17, 20] for rigorous studies of such waiting-time phenomena for (1.1a)). For $\alpha = 4/n$ an upper bound on t_w can be deduced from the local behaviour of the solution (cf. [29] for the corresponding case (1.6)); more generally, information about t_w can be obtained from the full (global) solution (cf. [28] for (1.6)).

(ii) For α below the critical value the interface will move at once, with (in view of (1.2)–(1.3))

$$s(t) > x_0 \quad \text{for } t > 0,$$

for $3/2 \leq n < 3$ (cf. [22] for (1.6)). For $n < 3/2$, however, $\dot{s} < 0$ is also possible so a further classification is required according to whether $\dot{s} > 0$ or $\dot{s} < 0$ for small $t > 0$. This does not arise in the corresponding analysis of (1.6) since $\dot{s} \geq 0$ necessarily holds.
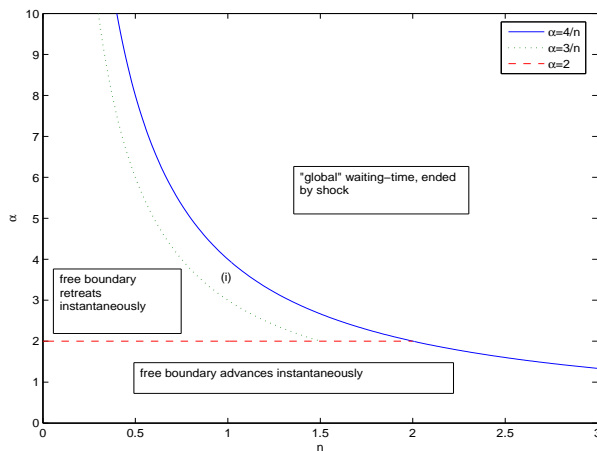

FIG. 1.1. *A summary of the possible small-time behaviours with respect to n and α. In region (i) a diverse range of waiting-time scenarios are seen (see §4 for details); by "shock", we mean that a large bulk of fluid suddenly overruns the interface.*

In addition, the higher order of (1.1a) leads, as we shall see, to a much more diverse range of waiting-time scenarios than that which occurs for (1.6).

In seeking a physical explanation for these results, we remark that large n implies high viscosity (less slip), and large α a shallow initial contact angle. Broadly speaking, the larger the value of n/α, the stronger is the tendency of solutions to stay positive. We are not aware of any experimental evidence to support our conjectures, but in light of our results such experiments might be timely. Instead, we support our asymptotic conjectures with numerical results. Without loss of generality we assume that $s(0) > 0$ and, for numerical purposes, we first approximate (1.1a–c) by replacing (1.1c) by

$$\frac{\partial h}{\partial x} = h^n \frac{\partial^3 h}{\partial x^3} = 0 \quad \text{for } x = 0, l, \tag{1.7c}$$

where $l \gg s(0)$, and restrict (1.1a) to hold on $(0, l)$. Existence of solution concepts for (1.1a,b), (1.7c) may be found in [5, 9, 14] and the references cited therein.

As described in [2] we discretise (1.1a,b), (1.7c) using finite elements in space and finite differences in time, using uniform spatial and temporal discretisation parameters

δx and δt, respectively; see §2 for details. We expect this method to be able to compute the zero contact angle solution for the following reasons:

1. In [5], the existence of solutions to (1.1a,b), (1.7c) is proved for $0 < n < 3$, where $h(\cdot, t)$ may be $C^1([0, l])$ for almost every $t > 0$ (the zero contact angle solution), or alternatively $h(\cdot, t)$ may have non-expansive support.
2. In [2] it was proved that the numerical solution converges, as $\delta x, \delta t \to 0$, to a weak solution of (1.1a,b), (1.7c) (in the sense of [5, 9, 14]). The only remaining question is whether this is the zero contact angle solution, or a solution with non-expansive support.
3. In a sequence of experiments, taking $\delta t = O(\delta x^{\frac{1}{2}})$, the numerical method computes a solution with non-expansive support.
4. In a sequence of experiments, taking $\delta t = O(\delta x^2)$, the numerical method can compute solutions where $|\dot{s}(0)| = \infty$ (zero contact angle solutions).
5. In [2] a self-similar source type solution was successfully computed with $\delta t = O(\delta x^2)$. Moreover, taking a non-smooth stationary solution as initial data, i.e. $h_0(x) = \alpha \max\{\gamma^2 - x^2, 0\}$ and $0 < \gamma < l$, the numerical method computed a smooth solution for $0 < n < 3$ and it was concluded that $h(x, t) \equiv h_0(x)$ for $n > 3$.

Hence in our experiments, in order to be sure that we are approximating the zero contact angle solution we always choose $\delta t = O(\delta x^2)$. We report that the numerical solution always appeared to be smooth.

An outline of the paper is as follows. We begin in §2 by describing our numerical scheme in more detail. We then proceed in §3 and §4 with a formal asymptotic analysis, supported by numerical experiments, for the two cases $\alpha \geq 4/n$ and $\alpha < 4/n$, respectively. Videos demonstrating more graphically how some of the numerical solutions of these sections evolve over time can be found online at

http://www.personal.rdg.ac.uk/~sms03sl/4thorder/4thorder.html

Finally in §5 we present some conclusions.

2. Numerical Approximation. Following the approach of [2], and as described in §1, we restrict (1.1a) to a finite space interval $(0, l)$, introduce a potential w and rewrite it as the system of equations

$$\frac{\partial h}{\partial t} = \frac{\partial}{\partial x}\left(h^n \frac{\partial w}{\partial x}\right) \quad \text{in } (0, l) \times (0, T), \tag{2.1a}$$

$$-\frac{\partial^2 h}{\partial x^2} = w \quad \text{in } (0, l) \times (0, T). \tag{2.1b}$$

A nonnegativity constraint is imposed on (2.1b) via a variational inequality in the weak form and then we discretise (2.1a,b) using the finite element method. Now given positive integers N and M, denote by $\delta t := T/M$ and $\delta x := l/N$ the temporal and spatial discretisation parameters, $t_k := k\delta t$, $k = 1, \ldots, M$, and $x_j = j\delta x$, $j = 0, \ldots, N$, then the discretisation may be written in the following way.

For $k = 1, \ldots, M$ and $j = 1, \ldots, N-1$ find $\{H_j^{k+1}, W_j^{k+1}\}$ such that

$$\frac{H_j^{k+1} - H_j^k}{\delta t} + \frac{1}{\delta x^2}\left[\int_{x_{j-1}}^{x_j}\left(\frac{(x - x_{j-1})}{\delta x}H_j^k + \frac{(x_j - x)}{\delta x}H_{j-1}^k\right)^n dx\right]\left(\frac{W_j^{k+1} - W_{j-1}^{k+1}}{\delta x}\right)$$

$$+ \frac{1}{\delta x^2}\left[\int_{x_j}^{x_{j+1}}\left(\frac{(x - x_j)}{\delta x}H_{j+1}^k + \frac{(x_{j+1} - x)}{\delta x}H_j^k\right)^n dx\right]\left(\frac{W_j^{k+1} - W_{j+1}^{k+1}}{\delta x}\right) = 0 \quad (2.2a)$$

$$\left[\frac{-H_{j+1}^{k+1} + 2H_j^{k+1} - H_{j-1}^{k+1}}{\delta x^2} - W_j^{k+1} \right] H_j^{k+1} = 0 \qquad (2.2b)$$

$$\frac{-H_{j+1}^{k+1} + 2H_j^{k+1} - H_{j-1}^{k+1}}{\delta x^2} - W_j^{k+1} \geq 0 \qquad (2.2c)$$

$$H_j^{k+1} \geq 0 \qquad (2.2d)$$

where $H_j^k \approx h(x_j, t_k)$, $W_j^k \approx w(x_j, t_k)$, $H_j^0 = h_0(x_j)$; similar equations/inequalities appropriate for boundary data (1.7c) hold for $j = 0, N$ when $k = 1, \ldots, M$. This non-linear system is solved using a Gauss-Seidel algorithm in multigrid mode; for details we refer to [3]. We found this approach to have several advantages over some other algorithms previously proposed in the literature, such as the Uzawa type algorithm [2, (3.7a–c)], [21]. Specifically:

1. If $H_{j-1}^k = H_j^k = H_{j+1}^k = 0$ then it follows from (2.2a) that $H_j^{k+1} = H_j^k = 0$, so that the free boundary advances at most one mesh point from time level k to time level $k+1$. The advantage of using the non-symmetric Gauss-Seidel smoother is that this constraint is easier to impose on the numerical method than with a symmetric smoother.

2. Working within a multigrid framework significantly increases the rate of convergence. This allows us to reduce the tolerance for the stopping criterion of the iterative scheme (the maximum absolute difference in successive iterates is smaller than tol) to $tol = 10^{-12}$, as compared with $tol = 10^{-8}$ in [2], and therefore to solve the nonlinear system more accurately, thereby helping to avoid spurious behaviour.

3. Non-negativity of the computed numerical solution is guaranteed, so defining the position x_c^k of the numerical free boundary at time t_k to be

$$x_c^k := \{x_j > 0 : H_m^k \leq \epsilon \text{ for all } m \geq j, \ H_{j-1}^k > \epsilon\}$$

we take $\epsilon = 0$ which tracks the free boundary more accurately than with $\epsilon > 0$, this compares with $\epsilon = 10^{-6}$ in [2]. We remark that because the numerical free boundary is defined on a discrete set of points, its movement appears to "stutter" in the figures below.

In the numerical experiments of §3 and §4 we solve (1.1a,b), (1.7c) with $l = 1$ and

$$h_0(x) = 5 \max \left\{ \left(\tfrac{9}{16} - x^2 \right)^\alpha, 0 \right\}; \qquad (2.3)$$

the key properties are that the maximum value of h_0 is $O(1)$ and the thin-film is symmetrically distributed about 0 with $x_0 = 3/4$. These experiments were performed for a sequence of space steps δx where $\delta t = C_{\alpha,n} \delta x^2$ and convergence of (2.2a)–(2.2d) to a weak solution of (1.1a,b), (1.7c), (2.3) was assured (see [2]). For reasons of space we refer to [15] for further figures and numerical results, including results from many more experiments with values of n and α closer to the edges of the parameter regimes.

3. Formal asymptotic analysis and numerical results for $\alpha \geq 4/n$. For $\alpha \geq 4/n$, the formal asymptotic analysis of this section suggests that we might expect waiting-time behaviour. In particular, for $\alpha > 4/n$ (§3.1) we anticipate "global" waiting-time behaviour, by which we mean that the asymptotic expansion tells us to expect a waiting-time, but gives no clue as to the local behaviour; in this case the interface starts to move due to "shock" formation, with the gradient becoming

unbounded near the free boundary. For $\alpha = 4/n$ (§3.2) this global breakdown can occur for the full range $0 < n < 3$, but for $2 < n < 3$ "local" waiting-time behaviour is also possible; by this we mean that the dominant term in the asymptotic expansion switches at the end of the waiting-time.

3.1. $\alpha > 4/n$: **"global" waiting-time behaviour.** Provided $h_0(x)$ is analytic away from the interfaces, then the small-time expansion

$$h \sim h_0 - \frac{\mathrm{d}}{\mathrm{d}x}\left(h_0^3 \frac{\mathrm{d}^3 h_0}{\mathrm{d}x^3}\right) t \quad \text{as } t \to 0^+ \tag{3.1}$$

holds, at least away from the interface. From (1.5) we have

$$\frac{\mathrm{d}}{\mathrm{d}x}\left(h_0^n \frac{\mathrm{d}^3 h_0}{\mathrm{d}x^3}\right) \sim \alpha(\alpha-1)(\alpha-2)((n+1)\alpha-3)A_0^{n+1}(x_0-x)^{(n+1)\alpha-4}$$
$$+ \left(n\alpha(\alpha-1)(\alpha-2) + \beta(\beta-1)(\beta-2)\right)(n\alpha+\beta-3)A_0^n C_0 (x_0-x)^{n\alpha+\beta-4}$$
$$\text{as } x \to x_0^-; \tag{3.2}$$

for $\alpha > 4/n$ we have $(n+1)\alpha - 4 > \alpha$, and we may expect the local behaviour

$$h \sim A_0(x_0-x)^\alpha \quad \text{as } x \to x_0^- \tag{3.3}$$

to hold up to some finite time $t = t_w > 0$, implying a waiting-time scenario in which the local behaviour at the interface does not change for some non-zero waiting-time.

To test this conjecture, we ran numerical experiments for a large range of n and $\alpha > 4/n$, considering in particular $n = 0.75$, 1.0, 1.75 and 2.5, so as to cover all of the different regimes important in the case $\alpha < 4/n$ (see §4).

In the upper left plot of Figure 3.1 we plot x_c^k against t_k for $n = 1.75$ and $\alpha = 3.0 > 4/n = 2.29$. The numerical free boundary remains stationary for a period before advancing. We also plot profiles of H_j^k in the vicinity of the interface at times just before and just after x_c^k begins to move (lower left plot). Shock-type behaviour at the end of the waiting-time can be observed (cf. [28] for the second-order case).
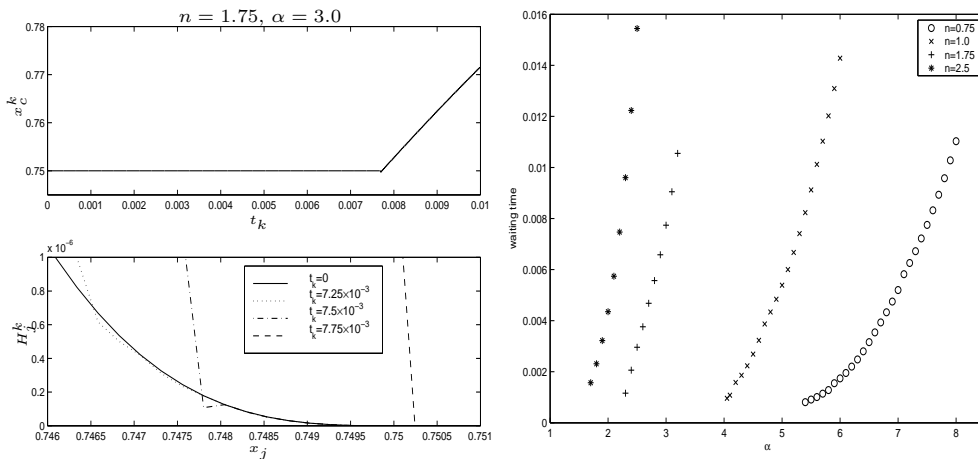

FIG. 3.1. *Waiting-time behaviour, various n, α.*

Similar waiting-time behaviour, with shock type behaviour at the end of the waiting-time, was observed for all n, α combinations tested in this range. Approximate waiting times are plotted against α in the right half of Figure 3.1, for

$n = 0.75, 1.0, 1.75, 2.5$ and for various $\alpha > 4/n$. For fixed n, the waiting time increases as α increases.

3.2. $\alpha = 4/n$: "local" waiting-time behaviour for $2 < n < 3$. In the critical case, the leading term in (1.5) suggests the separable local behaviour

$$h \sim \Lambda(t)(x_0 - x)^{4/n} \quad \text{as } x \to x_0^-,\tag{3.4}$$

with (1.1a–c) implying

$$\dot{\Lambda} = -\tfrac{4}{n}\left(\tfrac{4}{n} - 1\right)\left(\tfrac{4}{n} - 2\right)\left(\tfrac{4}{n} + 1\right)\Lambda^{n+1}.$$

Hence if $n \neq 2$ (recalling that we consider in this paper only $0 < n < 3$),

$$\Lambda = A_0\left(1 + \frac{8(4-n)(2-n)(n+4)A_0^n t}{n^3}\right)^{-\frac{1}{n}}.\tag{3.5}$$

This local solution also represents waiting-time behaviour; (3.5) blows up in finite time if $2 < n < 3$, so the waiting-time t_w then satisfies

$$t_w \leq t_c \equiv \frac{n^3}{8(4-n)(n-2)(n+4)A_0^n};$$

$\Lambda(t)$ decreases with time for $0 < n < 2$, but we nevertheless expect (3.4) to remain valid only up to some finite t_w, after which the front begins to move due to shock, as described in §3.1. Thus for $2 < n < 3$ local waiting-time behaviour ($t_w = t_c$) is possible, analogous to that for the porous-medium equation ([29]), while global breakdown ($t_w < t_c$ for $2 < n < 3$) can occur for the full range $0 < n < 3$ (cf. [28]).

4. Formal asymptotic analysis and numerical results for $\alpha < 4/n$. We begin in §4.1 by deriving some local similarity solutions. Based on these and the local behaviour indicated in (1.2)–(1.4), we conjecture in §4.2–§4.6 some parameter regimes for the small-time behaviour when $\alpha < 4/n$, in which case (3.3) fails for any $t > 0$. This does not mean that for $\alpha < 4/n$ there is no waiting-time behaviour; on the contrary, unlike for the corresponding second-order problem (1.6), a diverse range of waiting-time scenarios can occur in this case. In addition to these waiting-time scenarios, the front may also advance or retreat instantaneously. Many of our conjectures are supported by extensive numerical verifications, detailed below; we leave open their rigorous confirmation.

4.1. Local similarity solutions. In view of (1.5), a natural conjecture for the small-time behaviour for $\alpha < 4/n$ (balancing the terms in the expansion so they are of the same size) is the self-similar form

$$h \sim t^{\frac{\alpha}{4-n\alpha}} f\left((x - x_0)/t^{\frac{1}{4-n\alpha}}\right), \quad s(t) \sim x_0 + \eta_0 t^{\frac{1}{4-n\alpha}},\tag{4.1}$$

where with $\eta := (x - x_0)/t^{1/(4-n\alpha)}$, $f(\eta)$ satisfies the boundary-value problem

$$\frac{1}{4-n\alpha}\left(\alpha f - \eta \frac{df}{d\eta}\right) = -\frac{d}{d\eta}\left(f^n \frac{d^3 f}{d\eta^3}\right),\tag{4.2}$$

$$\text{as } \eta \to -\infty \quad f \sim A_0(-\eta)^\alpha - \alpha(\alpha-1)(\alpha-2)((n+1)\alpha-3)A_0^{n+1}(-\eta)^{(n+1)\alpha-4},\tag{4.3a}$$

$$\text{at } \eta = \eta_0 \quad f = \frac{df}{d\eta} = f^n \frac{d^3 f}{d\eta^3} = 0.\tag{4.3b}$$

Here $s(t)$ is the position of the contact line at time t, and η_0 is a free constant determined by the boundary-value problem.

The behaviour as $\eta \to -\infty$ in (4.3a) thereby matches via (3.1) with the leading terms in (1.5) and (3.2). The constant A_0 can be scaled out by setting

$$f = A_0^{\frac{4}{4-n\alpha}} \hat{f}, \quad \eta = A_0^{\frac{n}{4-n\alpha}} \hat{\eta},$$

suggesting in particular the delicacy of the limit $\alpha \to (4/n)^-$, and the transformation

$$f = |\eta|^{\frac{4}{n}} g(\xi), \quad \xi = \ln |\eta|$$

enables (4.2) to be reduced to a fourth-order autonomous problem. Nevertheless, the complexities of the resulting four-dimensional phase space mean that a global analysis of (4.2) (akin to that in [29] for the second-order problem) is not practicable here. Instead we base our conjectures in large part on a number of closed-form solutions to (4.2) which we now note. We assume (4.2)–(4.3a,b) to have a unique non-negative solution.

(I) Separable solution

$$f(\eta) = \left(\frac{n^3}{8(4-n)(2-n)(n+4)} (-\eta)^4 \right)^{\frac{1}{n}} \tag{4.4}$$

is an explicit solution to (4.2) for $0 < n < 2$, providing a possible local behaviour as $\eta \to 0^-$ for solutions with $\eta_0 = 0$; the circumstances under which (4.4) may be applicable are clarified in Appendix A.

(II) Steady state solution

$$f(\eta) = A_0(-\eta)^2, \quad \eta_0 = 0, \tag{4.5}$$

gives the solution to (4.2)–(4.3a,b) when $\alpha = 2$.

(III) Travelling wave solution

$$f(\eta) = A_0(\eta_0 - \eta)^{\frac{3}{n}}, \quad \eta_0 = \frac{3(3-n)(2n-3)A_0^n}{n^3}, \tag{4.6}$$

is the solution to (4.2)–(4.3a,b) when $\alpha = 3/n$, $n \neq 3/2$; here $\eta_0 > 0$ if $3/2 < n < 3$ and $\eta_0 < 0$ if $0 < n < 3/2$.

To complete our catalogue of pertinent closed form solutions we note that for $n = 1$ the polynomial solution (cf. [25])

$$h = \frac{A_0^3}{4(1 + 30C_0^2 t/A_0)C_0^2} \left((1 + C_0(x_0 - x)/A_0)^2 - (1 + 30C_0^2 t/A_0)^{\frac{2}{5}} \right)^2,$$

$$s = x_0 - A_0 \left((1 + 30C_0^2 t/A_0)^{\frac{1}{5}} - 1 \right)/C_0, \tag{4.7}$$

corresponds to

$$h_0 = A_0(x_0 - x)^2 + C_0(x_0 - x)^3 + C_0^2(x_0 - x)^4/(4A_0) \tag{4.8}$$

so that $\alpha = 2$, $\beta = 3$ in (1.5); hence s initially decreases if $C_0 > 0$ but increases if $C_0 < 0$, with

$$s(t) \sim x_0 - 15C_0 t \quad \text{as } t \to 0^+, \tag{4.9}$$

this dependence on the sign of C_0 being perhaps counter-intuitive, which is far from unusual in such high-order diffusion problems.

4.2. Small-time behaviour for 2 < n < 3. In this regime, the solution (4.4) is not available to describe the local behaviour of $f(\eta)$ at the interface; (4.6) has the expected local behaviour (1.2), while (4.5) corresponds to $\alpha > 4/n$ and therefore lies in the waiting-time regime discussed in §3.1. We thus anticipate that for any $\alpha < 4/n$ the support of h expands immediately according to (4.1) with $\eta_0 > 0$ and, in (4.2)–(4.3a,b),

$$f(\eta) \sim \left(\frac{n^3 \eta_0}{3(3-n)(2n-3)(4-n\alpha)} (\eta_0 - \eta)^3 \right)^{\frac{1}{n}} \quad \text{as } \eta \to \eta_0^-, \qquad (4.10)$$

which follows from (1.2). The interface advances with unbounded initial velocity for $\alpha < 3/n$, with finite positive initial velocity if $\alpha = 3/n$ (with $f(\eta)$ given by (4.6)) and with velocity tending to zero as $t \to 0^+$ for $\alpha > 3/n$. The behaviour in this regime is very much analogous to that exhibited by the porous-medium equation (cf. [22]).

To test this conjecture we ran numerical experiments for $n = 2.5$, for which $3/n = 1.2$ and $4/n = 1.6$, and for $\alpha \in [0.5, 1.5]$. Our results support the conjecture. In each case x_c^k advances, with the speed of the advance decreasing as α increases from 0.5 to 1.5. We plot x_c^k against t_k for $n = 2.5$ and for $\alpha = 0.5 < 3/n$ and $\alpha = 1.4 > 3/n$ in the upper half of Figure 4.1. Note the different time scales on the two plots.
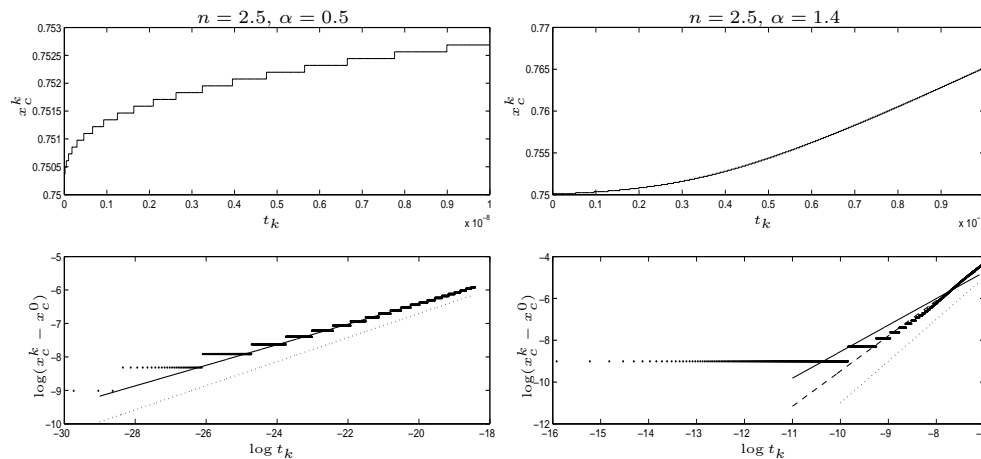

FIG. 4.1. *Numerical results for $n = 2.5$, $\alpha = 0.5$, $T = 10^{-8}$ (left), and for $n = 2.5$, $\alpha = 1.4$, $T = 10^{-3}$ (right). In the upper half of the figure the advancing free boundary is shown. In the lower half of the figure $\log t_k$ is plotted against $\log(x_c^k - x_c^0)$ as a discrete set of points, with the solid line following from a least squares fitting, the straight dotted line from asymptotic theory, and the dashed line in the lower right section following from a least squares fitting with the early data removed.*

In the lower half of Figure 4.1 we test the hypothesis that for small times

$$x_c^k = x_c^0 + A t_k^\gamma, \qquad (4.11)$$

for some constants $A > 0$ and γ, by plotting $\log(x_c^k - x_c^0)$ against $\log t_k$ (as a discrete set of points - these appear to "stutter" since the numerical free boundary advances by one discrete mesh point at a time). If the hypothesis is correct we expect a straight line with slope γ. To estimate the value of γ we take a least squares fit. For presentational purposes we plot the best fitting least squares line as a solid line, and for comparison we also plot a dotted line with slope $(4 - n\alpha)^{-1}$, the expected value of γ (recall (4.1)).

For $\alpha = 0.5$ the log-log plot is fairly straight, and the estimated value of $\gamma = 0.31$ is close to the expected value of 0.36. For $\alpha = 1.4$ the best fitting least squares line gives an estimate of $\gamma = 1.27$, which is not close to the expected value of 2.00, and is a poor fit to the data. In this case the immediate yet slow advance of the free boundary means that for t_k small, x_c^k overestimates the exact position of the free boundary. This is demonstrated by the fact that the lowest horizontal line of dots on the log-log plot, corresponding to the first step in the advance of x_c^k, matches very poorly with the rest of the data. In the lower right plot of Figure 4.1 we thus also show as a dashed line the best fitting least squares approximation to the data with the first step in the advance of x_c^k excluded (equivalently taking $t_k \gtrsim 5 \times 10^{-5}$ rather than $t_k > 0$ on the log-log plot). This dashed line, with a slope of 1.69, matches the slope of the data and the expected value of γ much more closely than our original estimate.

The expected and estimated values of γ for each value of α tested are shown in Table 4.1. For $\alpha \leq 1.3$ we estimate γ using all of the data, but for $\alpha = 1.4$ and $\alpha = 1.5$ we exclude the first step in the advance of x_c^k, as discussed above. The numerical results give a value of γ slightly lower than the expected value, but the difference is small, and the trend of γ increasing with α is clear. Our estimate for γ is more accurate for values of α away from the edges of the parameter regime.

α	0.5	0.6	0.7	0.8	0.9	1.0	1.1	1.2	1.3	1.4	1.5
$\frac{1}{4-n\alpha}$	0.36	0.40	0.44	0.50	0.57	0.67	0.80	1.00	1.33	2.00	4.00
γ	0.31	0.35	0.39	0.46	0.53	0.61	0.76	0.91	1.12	1.69	3.43

TABLE 4.1
Estimated and expected values of γ for $n = 2.5$, various α.

4.3. Small-time behaviour for n = 2. The behaviour for $\alpha < 2$ is as described in §4.2. However, for $\alpha = 2$ the solution (4.1) is not applicable and, partly because $\alpha = 2$ will also play an important role in what follows, additional comments regarding the resulting waiting-time scenario are instructive. The small-time solution (4.5) suggests that there is initially no change in local behaviour, while (3.2) becomes

$$\frac{\mathrm{d}}{\mathrm{d}x}\left(h_0^n \frac{\mathrm{d}^3 h_0}{\mathrm{d}x^3}\right) \sim (\beta + 1)\beta(\beta - 1)(\beta - 2)A_0^2 C_0 (x_0 - x)^\beta t; \qquad (4.12)$$

both suggest seeking a local solution of the form

$$h \sim A_0(x_0 - x)^2 + H(x, t) \quad \text{as } x \to x_0^-; \qquad (4.13)$$

we note that H need not be positive on $x < x_0$ because it represents a correction term to the (quadratic) leading order behaviour. Linearising in H yields

$$\frac{\partial H}{\partial t} = -A_0^2 \frac{\partial}{\partial x}\left((x_0 - x)^4 \frac{\partial^3 H}{\partial x^3}\right)$$

so, given (1.5) in which $\beta > 2$ is required, the correction term takes the separable form

$$H = C_0(x_0 - x)^\beta \exp\left(-(\beta + 1)\beta(\beta - 1)(\beta - 2)A_0^2 t\right),$$

consistent with (3.1), (4.12). The perturbation to the quadratic term thus decays exponentially and we expect (4.13) to persist up to some finite waiting-time, after which the interface will start to move due to "shock" formation (as in other "global" waiting-time cases described here; see [28] for the second-order analogue).

4.4. Small-time behaviour for $3/2 < n < 2$. In this case (4.6) again has the expected interface behaviour (1.2), while (4.5) is non-generic in the sense that it is smoother than (1.2) at the interface; the solution of (4.2)–(4.3a,b) for $\alpha = 2$ is therefore an exceptional connection in phase space and can be expected to play a role in separating distinct regimes, as we now suggest. The other noteworthy change to occur as n drops below two is that the local behaviour (4.4) can come into play.

4.4.1. $2 < \alpha < 4/n$. The solution to (4.2)–(4.3a,b) has the local behaviour which decays as $(-\eta)^{4/n}$ as $\eta \to 0^-$ and exhibits a finite waiting time; for $\alpha_2 < \alpha < 4/n$, where α_i, $i = 1, 2, 5$ are defined in Appendix A, $f(\eta)$ has local behaviour (4.4), so the solution decreases such that

$$h \sim \left(\frac{n^3(x_0 - x)^4}{8(4-n)(2-n)(n+4)t} \right)^{1/n} \quad \text{as } x \to x_0^-, \ 0 < t < t_w \qquad (4.14)$$

for the duration of the period of waiting. Moreover, for $\alpha_5 < \alpha < 4/n$, we expect non-oscillatory decay, whereas for $\alpha_2 < \alpha < \alpha_5$ we expect damped oscillations to occur. See Appendix A for details. For $2 < \alpha < \alpha_2$ the behaviour is slightly more subtle, with a limit cycle (see (A.5) of Appendix A) arising in the local description for $0 < t < t_w$; the limiting behaviour as $\alpha \to 2$ is addressed in Appendix B, providing additional support for conjectures about the (rather subtle) asymptotic behaviour.

We present numerical results for $n = 1.75$ (giving $3/n = 1.7143$, $\alpha_2(n) = 2.0768$, $\alpha_5(n) = 2.2$, $4/n = 2.2857$), and for $\alpha = 2.24$, 2.10 and 2.04, thus covering each of the three parameter regimes described above. In the upper left plots of Figures 4.2, 4.3 and 4.4, we plot x_c^k against t_k for $n = 1.75$ and $\alpha = 2.24$, 2.10 and 2.04 respectively. In each case x_c^k remains stationary for a period before advancing, with the length of the waiting period appearing to decrease as α decreases. We also plot in each figure profiles of H_j^k near the interface at various times whilst the free boundary is stationary (upper right plot), and just as the free boundary is beginning to advance (lower left plot). In each case as $x \to x_0^-$ the profile of H_j^k appears to remain unchanged for a short waiting period. In the lower right plot of each figure we plot $\log H_j^k$ against $\log(0.75 - x_j)$ in the vicinity of the free boundary at the same times and using the same legend as in the upper right plot of each figure, plotting also a dotted line with slope $4/n$ for comparison.

For $\alpha = 2.24$ (Figure 4.2) the (nearly) straight lines with slopes 2.26 for $t_k = 2.5 \times 10^{-4}$ and 2.29 for $t_k = 5.0 \times 10^{-4}$ (estimated as before) compare well with the value of $4/n = 2.29$ proposed in the conjecture. For $t_k = 7.5 \times 10^{-4}$ the log-log plot is no longer straight, and the best fitting least squares line has a slope of 2.47; by this time the profile of H_j^k has begun to change.

For $\alpha = 2.10$ (Figure 4.3), the (nearly) straight lines have slopes 2.17 for $t_k = 2.5 \times 10^{-4}$ and 2.18 for $t_k = 5.0 \times 10^{-4}$. These values are slightly lower than for $\alpha = 2.24$, but still compare fairly well with the value of $4/n = 2.29$ proposed in the conjecture. For $t_k = 7.5 \times 10^{-4}$ again the log-log plot is no longer straight, and the best fitting least squares line has a slope of 1.27; by this time the profile of H_j^k has again begun to change.

For $\alpha = 2.04$ (Figure 4.4) each log-log plot is again (nearly) a straight line, however the slopes of 2.09 for $t_k = 2.0 \times 10^{-4}$ and 2.08 for $t_k = 3.0 \times 10^{-4}$ are somewhat smaller than the value of $4/n = 2.29$. As t_k increases from zero, the slope of the log-log plot increases from 2.04 up to a maximum of 2.09 before decreasing. For $t_k = 4.0 \times 10^{-4}$ the line has a slope of 1.91; by this time the profile of H_j^k has begun to change noticeably.
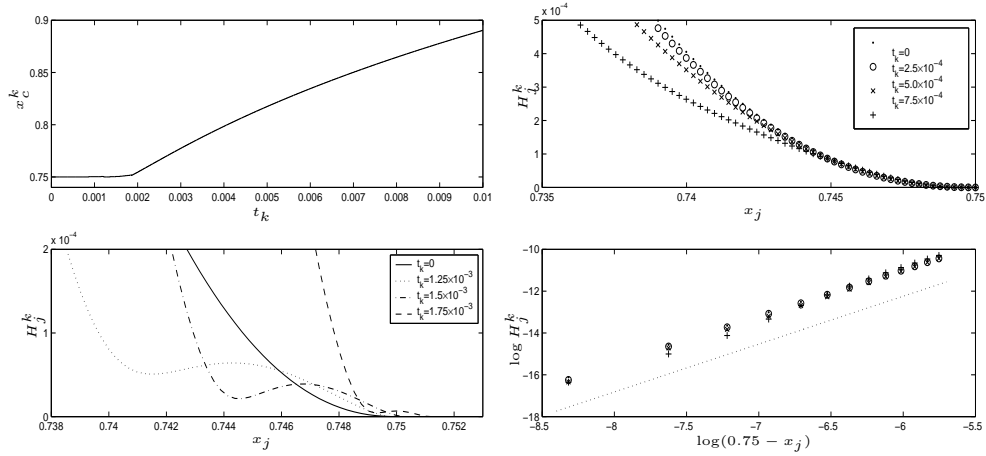
FIG. 4.2. *Numerical results for $n = 1.75$, $\alpha = 2.24$; waiting-time behaviour (upper left plot); profiles of H_j^k near the interface whilst the free boundary is stationary (upper right plot), and as the free boundary advances (lower left plot); $\log H_j^k$ against $\log(0.75 - x_j)$ in the vicinity of the free boundary, with a dotted line from asymptotic theory (lower right plot - same legend as upper right).*
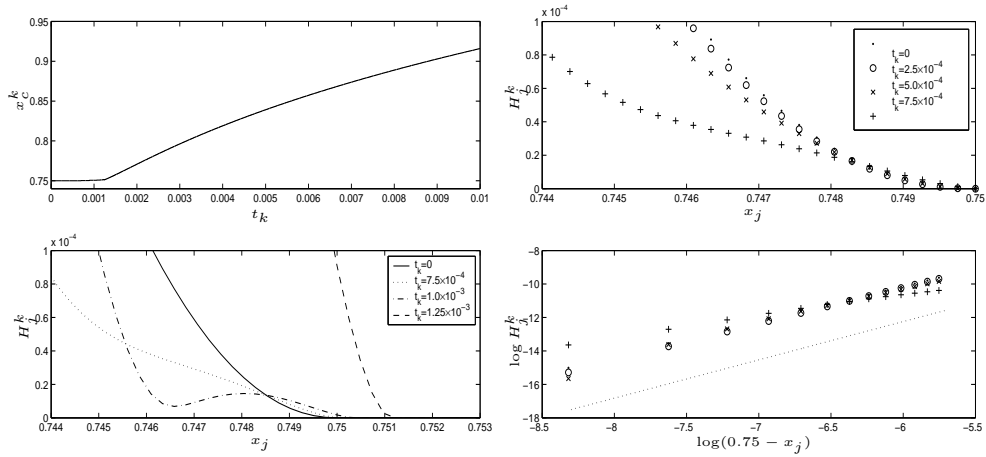

FIG. 4.3. *Numerical results for $n = 1.75$, $\alpha = 2.10$; waiting-time behaviour (upper left plot); profiles of H_j^k near the interface whilst the free boundary is stationary (upper right plot), and as the free boundary advances (lower left plot); $\log H_j^k$ against $\log(0.75 - x_j)$ in the vicinity of the free boundary, with a dotted line from asymptotic theory (lower right plot - same legend as upper right).*

4.4.2. $\alpha = 2$. This is the most delicate case, with the small-time behaviour depending on the correction term in (1.5), with $\beta > 2$. In (3.2) we have

$$\frac{\mathrm{d}}{\mathrm{d}x}\left(h_0^n \frac{\mathrm{d}^3 h_0}{\mathrm{d}x^3}\right) \sim \beta(\beta - 1)(\beta - 2)(2n + \beta - 3)A_0^n C_0 (x_0 - x)^{2n+\beta-4} \qquad (4.15)$$

and (4.13) yields

$$\frac{\partial H}{\partial t} = -A_0^n \frac{\partial}{\partial x}\left((x_0 - x)^{2n}\frac{\partial^3 H}{\partial x^3}\right), \qquad (4.16)$$
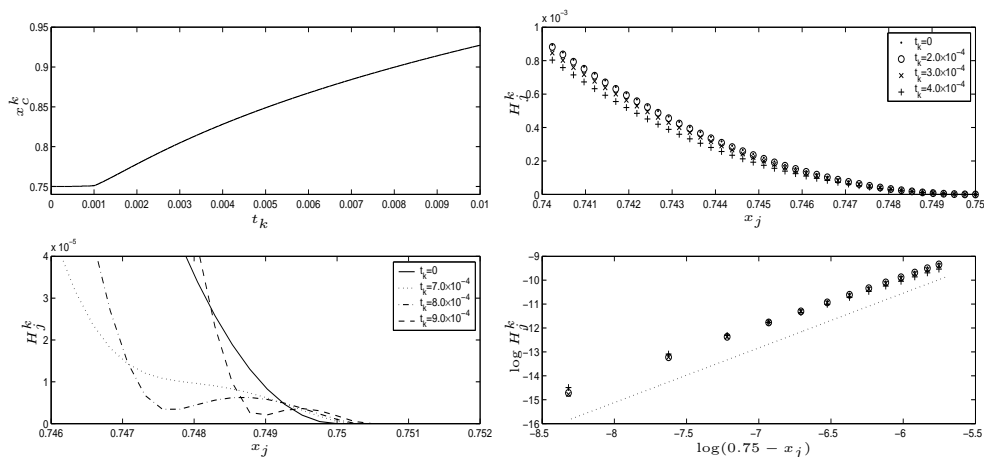
FIG. 4.4. *Numerical results for $n = 1.75$, $\alpha = 2.04$; waiting-time behaviour (upper left plot); profiles of H_j^k near the interface whilst the free boundary is stationary (upper right plot), and as the free boundary advances (lower left plot); $\log H_j^k$ against $\log(0.75 - x_j)$ in the vicinity of the free boundary, with a dotted line from asymptotic theory (lower right plot - same legend as upper right).*

implying, in view of (4.15), the small-time behaviour

$$H = A_0^{\frac{n\beta}{4-2n}} C_0 t^{\frac{\beta}{4-2n}} \Phi(\xi), \quad \xi = (x - x_0)/\left(A_0^{\frac{n}{4-2n}} t^{\frac{1}{4-2n}}\right)$$

being a similarity reduction of (4.16) in which $\Phi(\xi; n, \beta)$ is required to satisfy the matching conditions

$$\text{as } \xi \to -\infty \quad \Phi \sim (-\xi)^\beta - \beta(\beta - 1)(\beta - 2)(2n + \beta - 3)(-\xi)^{2n+\beta-4}$$

$$\text{at } \xi = 0^- \quad \Phi = (-\xi)^{2n}\frac{d^3\Phi}{d\xi^3} = 0,$$

from which it follows that

$$\Phi \sim \kappa(\beta, n)(-\xi) \quad \text{as } \xi \to 0^- \tag{4.18}$$

for some constant κ (which could in principle take either sign, reliable intuition about the signs of such quantities being hard to come by in high-order diffusion problems). In fact, for $\beta = 1 + 2(2 - n)N$ for integer N (such that $\beta > 2$), $\Phi(\xi)$ takes the form

$$\Phi = (-\xi) \sum_{m=0}^{N} a_m(-\xi)^{2(2-n)m}$$

with $a_N = 1$ and where a_0 alternates in sign with increasing N. More significantly, for $\beta = 2(1 + (2 - n)N)$, we have

$$\Phi = (-\xi)^2 \sum_{m=0}^{N} a_m(-\xi)^{2(2-n)m}$$

so that

$$\kappa(2(1 + (2 - n)N), n) = 0 \tag{4.19}$$

gives explicitly the values of β

$$\beta_N = 2(1 + (2 - n)N), \quad N = 1, 2, 3, \ldots \tag{4.20}$$

at which κ changes sign. Thus κ changes sign infinitely often as $\beta \to \infty$.

In view of (4.13) and (4.18) there is a further, narrower, inner region with

$$x = x_0 + t^{\frac{\beta-1}{4-2n}}\zeta, \quad h \sim t^{\frac{\beta-1}{2-n}}\Psi(\zeta), \tag{4.21}$$

the dominant balance as $t \to 0^+$ being given by

$$\frac{\mathrm{d}}{\mathrm{d}\zeta}\left(\Psi^n \frac{\mathrm{d}^3\Psi}{\mathrm{d}\zeta^3}\right) = 0,$$

implying

$$\frac{\mathrm{d}^3\Psi}{\mathrm{d}\zeta^3} = 0. \tag{4.22}$$

For $C_0\kappa > 0$ we thus have instantaneous advance of the interface (with velocity zero at $t = 0^+$) with

$$\Psi = A_0(\zeta_0 - \zeta)^2, \quad \zeta_0 = A_0^{\frac{n(\beta+1)-4}{4-2n}}C_0\kappa, \quad s \sim x_0 + \zeta_0 t^{\frac{\beta-1}{4-2n}}, \tag{4.23}$$

in order to match with (4.18). A yet narrower inner region, with

$$\zeta = \zeta_0 + O(t^{(\beta-2)/(2n-3)}),$$

is then present near the interface, with scalings

$$x = s(t) + t^{\frac{\beta-5+2n}{2(2-n)(2n-3)}}z, \quad h \sim t^{\frac{\beta-5+2n}{(2-n)(2n-3)}}\phi(z), \tag{4.24}$$

whereby, matching with (4.23),

$$\frac{\beta-1}{4-2n}\zeta_0 = \phi^{n-1}\frac{\mathrm{d}^3\phi}{\mathrm{d}z^3}, \tag{4.25a}$$

$$\text{as } z \to -\infty \quad \phi \sim A_0(-z)^2, \tag{4.25b}$$

$$\text{at } z = 0^- \quad \phi = \frac{\mathrm{d}\phi}{\mathrm{d}z} = 0. \tag{4.25c}$$

This completes the description of the case $C_0\kappa > 0$.

The problem (4.25a–c) has no solution for $\zeta_0 < 0$, corresponding to the fact that interfaces cannot recede when $n \geq 3/2$; a different scenario is therefore needed when $C_0\kappa < 0$ in which $\zeta = \zeta_0$ in (4.23) no longer coincides with the interface; in other words a quantity $\sigma(t)$, with

$$\sigma \sim x_0 + \zeta_0 t^{\frac{\beta-1}{4-2n}} \quad \text{as } t \to 0^+, \tag{4.26}$$

replaces $s(t)$ in (4.24) (with $s(t) = x_0$ now holding for $t \leq t_w$) and (4.25a–c) becomes

$$\frac{\beta-1}{4-2n}\zeta_0(\phi - \phi_\infty) = \phi^n\frac{\mathrm{d}^3\phi}{\mathrm{d}z^3}, \tag{4.27a}$$

$$\text{as } z \to -\infty \quad \phi \sim A_0(-z)^2, \tag{4.27b}$$

$$\text{as } z \to \infty \quad \phi \sim \phi_\infty, \tag{4.27c}$$

a boundary condition count indicating that, since $\zeta_0 < 0$, (4.27a–c) suffices to determine $\phi(z)$, up to translates in z, and ϕ_∞. The scaling properties of (4.27a–c) imply that ϕ and ϕ_∞ are proportional to $(\zeta_0^2/A_0^3)^{1/(2n-3)}$, with z scaling as $(|\zeta_0|/A_0^n)^{1/(2n-3)}$. In $\sigma < x < x_0$, whereby

$$x_0 - x = O\left(t^{\frac{\beta-1}{4-2n}}\right), \quad h = O\left(t^{\frac{\beta-5+2n}{(2-n)(2n-3)}}\right),$$

we have to leading order that $\partial h/\partial t = 0$ with, in view of (4.26)–(4.27a–c), the matching condition

$$h \sim ((x_0 - x)/|\zeta_0|)^{\widehat{\alpha}(\beta)} \quad \text{on } t = \sigma^{-1}(x),$$

where

$$\widehat{\alpha}(\beta) := \frac{2(\beta - 5 + 2n)}{(\beta - 1)(2n - 3)},$$

implying that

$$h \sim ((x_0 - x)/|\zeta_0|)^{\widehat{\alpha}(\beta)} \quad \text{for } \sigma < x < x_0. \tag{4.28}$$

The exponent $\widehat{\alpha}(\beta)$ in (4.28) is monotonic increasing in β (given that $\beta > 2$) and satisfies

$$\widehat{\alpha}(2) = 2, \quad \widehat{\alpha}\left(1 + \frac{2n}{3}\right) = \frac{4}{n}, \quad \widehat{\alpha}(\infty) = \frac{2}{2n-3}.$$

It follows for $\beta > 1 + 2n/3$ that $\widehat{\alpha}$ lies in the regime of §3.1, so that (4.28) describes the behaviour near the interface up to the waiting time; for $2 < \beta < 1 + 2n/3$, however, $\widehat{\alpha}$ lies in the regime of §4.4.1, so that (4.28) in turn breaks down sufficiently close to the interface and (4.14) is attained locally via a small-time similarity solution of the form (4.1)–(4.3a,b), with α replaced by $\widehat{\alpha}$. Such behaviour represents a novel waiting-time phenomenon for degenerate parabolic equations (there being no corresponding scenario for the porous-medium equation), but there are similarities with, for example, Hele-Shaw flows with suction, whereby the free surface profile can instantly change to a new configuration (cf. (4.28)), which then persists (see [26]).

Analysis of cases with $\kappa = 0$ requires specification of an additional term in the local (1.5) and remarkably fine structure in consequence arises. Thus (cf. (4.19)) for

$$h_0(x) \sim A_0(x_0 - x)^2 + C_0(x_0 - x)^{2(1+(2-n)N)} + D_0(x_0 - x)^\gamma \tag{4.29}$$

where $\gamma > 2(1 + (2 - n)N)$, we expect for each N a sequence of critical values of γ which represent further refined dividing lines between solutions which expand at once and those which wait; for those borderline values of γ, a further term in the expansion of (4.29) must be incorporated and so on. The first set of these dividing lines can be identified concisely via the one-degree-of-freedom (i.e. overspecified) family of local solutions (obtained by constructing an algebraic expansion for h about the leading order term in (4.30))

$$h \sim a(t)(x_0 - x)^2 - \frac{\dot{a}(t)}{12(2-n)(5-2n)(3-n)a^n(t)}(x_0 - x)^{6-2n} + O((x_0 - x)^{10-4n}), \tag{4.30}$$

corresponding to (4.29) with $N = 1$ and

$$a(0) = A_0, \quad \dot{a}(0) = -12(2 - n)(5 - 2n)(3 - n)A_0^n C_0,$$

and identifying the first critical value of γ for $N = 1$ to be $7 - 4n$; higher values of N correspond to $\dot{a}(0) = 0$ in this local expansion. Because it is overspecified, the local expansion of (4.30) pertains only when the local form of the initial data is consistent with the powers of $x_0 - x$ therein and, as already implied, it represents a borderline between solutions of the form (1.2) and (4.14).

4.4.3. $\alpha < 2$. Here the interface advances immediately, with $f(\eta)$ having local behaviour (4.10) and with unbounded initial velocity for $\alpha < 3/n$, finite for $\alpha = 3/n$ and tending to zero for $3/n < \alpha < 2$. The last of these ranges disappears as n drops below $3/2$, providing one indication of the need to address this regime separately.

To test this we ran numerical experiments for $n = 1.75$ (giving $3/n = 1.7143$, $4/n = 2.2857$), with $\alpha \in [0.5, 1.9]$. Our results again support the conjecture. In each case x_c^k advances, with the speed of the advance decreasing as α increases. This is shown in Figure 4.5, in which x_c^k is plotted against t_k for $n = 1.75$ with $\alpha = 0.5, 0.6$, 0.7 and 0.8 (upper left plot) and $\alpha = 1.6, 1.7, 1.8$ and 1.9 (lower left plot). Note the different time scales on the two axes.
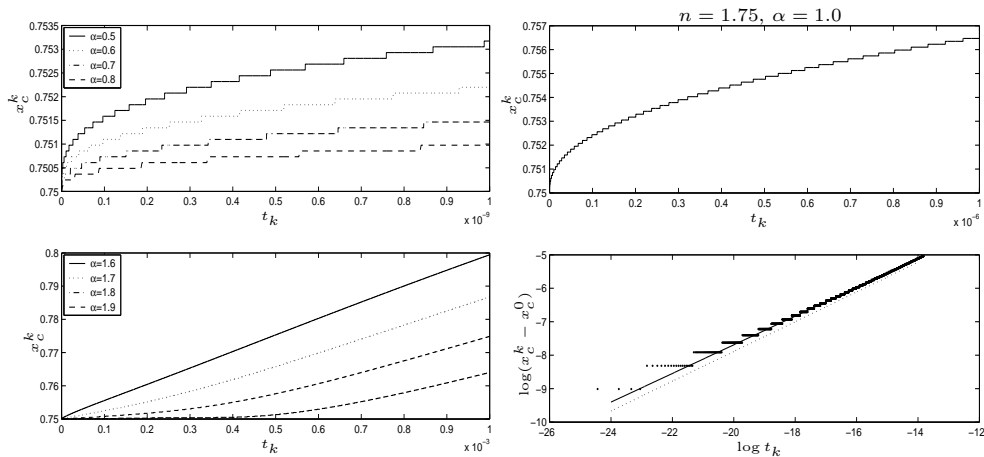

FIG. 4.5. *Numerical results for $n = 1.75$, $\alpha < 2$. On the left we show the numerical free boundary advancing for $\alpha = 0.5, 0.6, 0.7, 0.8$, $T = 10^{-9}$ (upper left plot) and for $\alpha = 1.6, 1.7, 1.8, 1.9$, $T = 10^{-3}$ (lower left plot); on the right we present results for $\alpha = 1.0$, $T = 10^{-6}$, with the numerical free boundary plotted against time in the upper right plot, and with $\log t_k$ plotted against $\log(x_c^k - x_c^0)$ as a discrete set of points in the lower right plot, with the solid line following from a least squares fitting and the straight dotted line from asymptotic theory.*

In the upper right plot of Figure 4.5 we show the numerical free boundary advancing for $n = 1.75$ and $\alpha = 1.0 < 3/n$. As before we test the hypothesis (4.11) by plotting $\log t_k$ against $\log(x_c^k - x_c^0)$ (in the lower right plot), and we estimate $\gamma = 0.43$. For comparative purposes we plot a dotted line with slope $(4 - n\alpha)^{-1} = 0.44$ on the same graph. The expected and estimated values of γ are shown in Table 4.2. For $\alpha = 1.9$ we exclude the first step in the advance of x_c^k, as discussed in §4.2. The estimates for γ are very close to the expected values, with this being especially true for values of α away from the edges of the parameter regime.

4.5. Small-time behaviour for $n = 3/2$. For $\alpha < 2$, the support of h expands immediately with unbounded velocity; in view of (1.3), the local behaviour of $f(\eta)$

α	0.5	0.7	0.9	1.1	1.3	1.5	1.7	1.9
$(4 - n\alpha)^{-1}$	0.32	0.36	0.41	0.48	0.58	0.73	0.98	1.48
γ	0.30	0.34	0.40	0.47	0.58	0.73	0.98	1.53

TABLE 4.2
Estimated and expected values of γ for various α, $n = 1.75$

then takes the form

$$f(\eta) \sim \left(\frac{3\eta_0}{2(8 - 3\alpha)}(\eta_0 - \eta)^3 \ln(1/(\eta_0 - \eta)) \right)^{\frac{2}{3}} \quad \text{as } \eta \to \eta_0^-.$$

For $2 < \alpha < 8/3$ the behaviour is again as described in §4.4.1. The case $\alpha = 2$ is particularly delicate, with the initial exponents $\alpha = 2$ and $\alpha = 3/n$ coinciding for $n = 3/2$. Much of the analysis in §4.4.2 nevertheless still pertains, in particular (4.18)–(4.20) hold, so that $\beta_N = 2 + N$, as does (4.21)–(4.23). However, the scalings (4.24) are evidently inapplicable for $n = 3/2$ and the appropriate scalings are instead (for $C_0\kappa > 0$)

$$h = (s - x)^2 \Phi(\xi, t), \quad \xi = t^{\beta - 2} \ln(1/(s - x)), \quad s \sim x_0 + \zeta_0 t^{\beta - 1}, \qquad (4.31)$$

so that the spatial scaling is exponentially small in t, which yield as dominant balance

$$(\beta - 1)\zeta_0 = 2\Phi_0^{1/2} \frac{d\Phi_0}{d\xi},$$

and hence

$$\Phi_0 = \left(A_0^{3/2} + \frac{3}{4}(\beta - 1)\zeta_0\xi \right)^{2/3} \qquad (4.32)$$

where we have matched with (4.23). For $C_0\kappa > 0$, this has the required local behaviour (1.3) and completes the small-time analysis. For $C_0\kappa < 0$, we again introduce

$$\sigma \sim x_0 + \zeta_0 t^{\beta - 1},$$

which specifies the interior layer location, and replace the scalings in (4.31) by

$$h = (\sigma - x)^2 \Phi(\xi, t), \quad \xi = t^{\beta - 2} \ln(1/(\sigma - x)),$$

to recover (4.32) with ζ_0 (given by (4.23)) negative. Hence ϕ_0 becomes zero at $\xi = \xi_c$, where

$$\xi_c = \frac{4A_0^{3/2}}{3(\beta - 1)|\zeta_0|}.$$

There is now a further asymptotic region in which

$$x = \sigma(t) + \rho(t)e^{-\xi_c/t^{\beta - 2}} z, \quad h \sim |\dot{\sigma}|^{2/3}\rho^2 e^{2\xi_c/t^{\beta - 2}} \phi, \qquad (4.33)$$

where the scaling on h is chosen to obtain the appropriate leading order balance, namely (cf. (4.27a–c))

$$-(\phi - \phi_\infty) = \phi^{3/2} \frac{d^3\phi}{dz^3},$$

$$\text{as } z \to -\infty \quad \phi \sim \left(\frac{3}{4}(-z)^3 \ln(-z) \right)^{2/3},$$

$$\text{as } z \to \infty \quad \phi \sim \phi_\infty,$$

where ϕ_∞ is again to be determined as part of the solution and we have matched with (4.32). The pre-exponential factor $\rho(t)$ is expected to be algebraic in t; its calculation would require correction terms in the various expansions to be evaluated and we shall not pursue such matters further. Applying similar arguments to those in §4.4.2 we obtain from (4.33) that

$$\ln h \sim -2\xi_c|\zeta_0|^{\frac{\beta-2}{\beta-1}}/(x_0 - x)^{\frac{\beta-2}{\beta-1}} \quad \text{for } \sigma < x < x_0, \tag{4.34}$$

so the height of the film left behind by the retreating interior layer at $x = \sigma$ is exponentially small (and thus in particular implies waiting-time behaviour at $x = x_0$). This reflects the status of $n = 3/2$ as a critical case; as we shall shortly see, for $n < 3/2$ the interface $x = s$ itself retreats in the corresponding regime (in other words, the film thickness left behind $x = \sigma$ drops from being algebraically small for $3/2 < n < 2$, as in (4.28), through exponentially small for $n = 3/2$ (see (4.34)) to zero for $n < 3/2$).

4.6. Small-time behaviour for n $<$ 3/2. We have already alluded to the qualitatively new feature, implicit in the local behaviour (1.4), which can occur in this regime, namely that the interface can retreat. Such behaviour is most simply demonstrated by the case $\alpha = 3/n$ in which the small-time similarity solution is given by (4.6), with the interface retreating at a finite rate; in this regime (4.6) is non-generic, being smoother than the expected local behaviour (1.4). For $\alpha > 3/n$, we anticipate waiting-time behaviour, as in §4.4.1; see also Appendix A (in addition an analysis similar to that of Appendix B can be performed in the limit $\alpha \to (3/n)^+$). The result for $\alpha = 3/n$ and $\alpha = 2$ suggests that for $\alpha < 2$ the interface expands at an unbounded rate, with

$$f(\eta) \sim \beta(\eta_0 - \eta)^2 \quad \text{as } \eta \to \eta_0^- \tag{4.35}$$

for some constant η_0, while for $2 < \alpha < 3/n$ contraction occurs at an unbounded rate, with $\eta_0 < 0$ in (4.35). The critical case $\alpha = 2$ is again of particular interest, in particular since waiting-time behaviour can in principle occur in this case also (but only for extremely special initial data, cf. (4.30)). The analysis for $\alpha = 2$ is more straightforward than that above, since (4.23)–(4.25a–c) now apply right up to the interface for $C_0\kappa < 0$ (retreat) as well as for $C_0\kappa > 0$ (advance). Such behaviour can be illustrated by the explicit solution (4.7)–(4.9) for $n = 1$, wherein $\beta = 3$ and $\kappa = -15$.

For $\alpha = 2$ we have that

$$s(t) \sim x_0 + \zeta_0 t^{\frac{\beta-1}{4-2n}} \quad \text{as } t \to 0^+;$$

which exhibits the same interface time-dependence as (4.1) with $\alpha = (4(\beta - 2) + 2n)/((\beta-1)n)$; since $\beta > 2$, it follows that this α lies in the range $2 < \alpha < 4/n$ and it implies that the same $s(t)$ can result from quite different initial data (in this case for $2 < \alpha < 3/n$, for which the interface retreats). This reflects the high order of (1.1a), whereby the local behaviour at the interface contains a further degree of freedom in addition to $s(t)$ and contrasts with the situation for the second-order case (1.6) (cf. [1]).

4.6.1. 3/n $<$ α $<$ 4/n. In this regime we anticipate waiting-time behaviour, as described in §4.4.1. For $\alpha_5 < \alpha < 4/n$ we expect monotonic decay onto the $4/n$ solution, for $\alpha_2 < \alpha < \alpha_5$ we expect oscillatory decay, and for $3/n < \alpha < \alpha_2$ we expect a limit cycle to arise in the local description for $0 < t < t_w$ (see (A.5)).

By monotonic decay we mean decay like $\eta^{-\gamma}$, where γ is real, and by oscillatory decay we mean that the solution decays like $\eta^{-\gamma - i\mu}$, where γ, μ are real. We present numerical results below for $n = 0.75$ (giving $3/n = 4$, $\alpha_2(n) = 4.2061$, $\alpha_5(n) = 4.9$, $4/n = 5.3333$), with $\alpha = 5.1$ (Figures 4.6 and 4.7), $\alpha = 4.5$ (Figures 4.8 and 4.9) and $\alpha = 4.1$ (Figures 4.10 and 4.11), thus covering each of the three parameter regimes described above (see also Appendix A). We also present results for $n = 1.0$ (for which $\alpha_2(n) = 3.2195$) with $\alpha = 3.1$ (Figures 4.12 and 4.13), with this second example in the range $3/n < \alpha < \alpha_2$ reflecting the extremely delicate nature of the results in this regime.
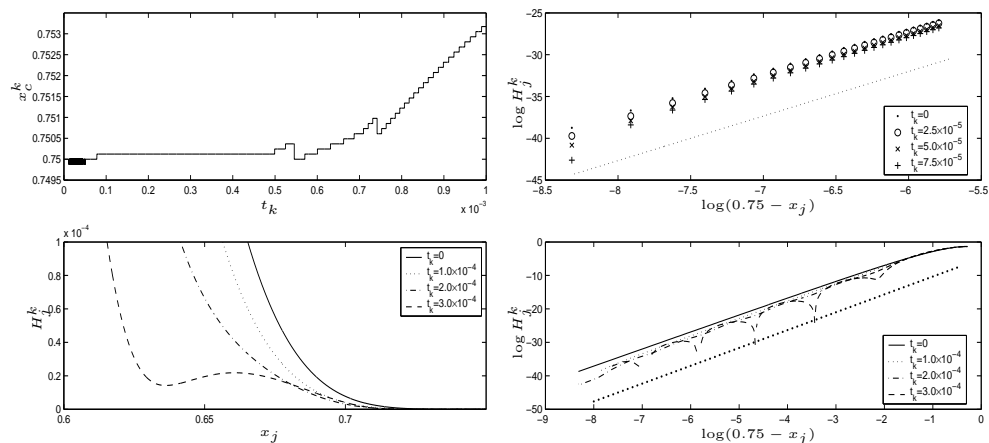
FIG. 4.6. *Numerical results for $n = 0.75$, $\alpha = 5.1$; waiting-time behaviour (upper left plot); profile of H_j^k near the interface at various times (lower left plot); $\log H_j^k$ against $\log(x_c^k - x_j)$ in the vicinity of the free boundary (upper right plot), and over the whole range $x_j \in [0, x_c^k)$ (lower right plot), with a dotted line of gradient $4/n$ (from asymptotic theory) in each case.*
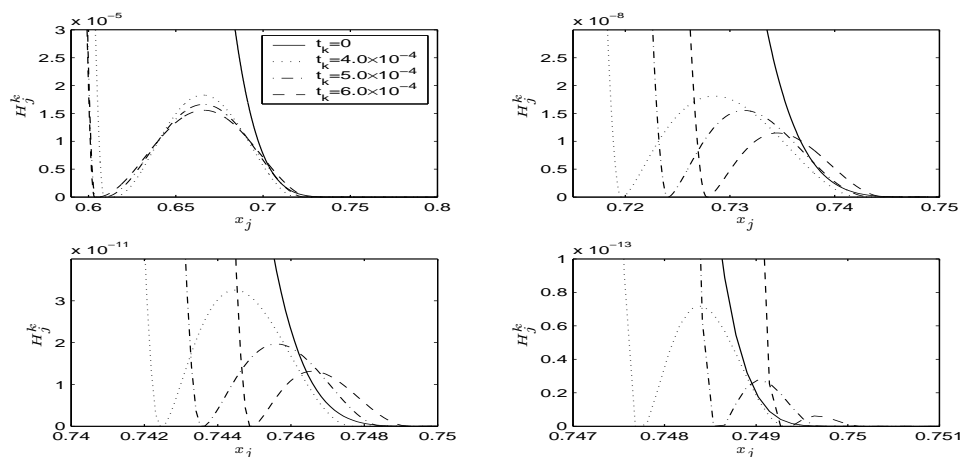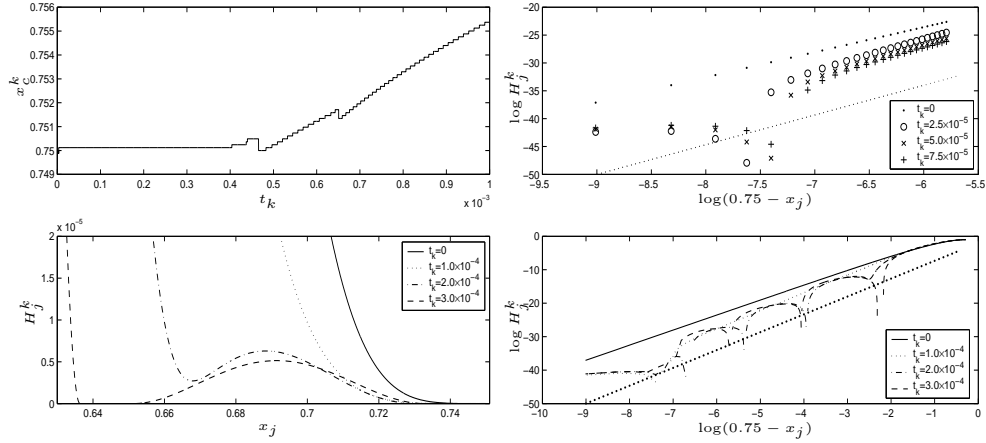

FIG. 4.7. *Numerical results for $n = 0.75$, $\alpha = 5.1$; profile of H_j^k near the interface at various times (same legend for each plot).*

In the upper left plots of Figures 4.6, 4.8, 4.10 and 4.12 we plot x_c^k against t_k for each example. In Figures 4.6 and 4.8, x_c^k remains stationary for a period before

FIG. 4.8. *Numerical results for* $n = 0.75$, $\alpha = 4.5$; *waiting-time behaviour (upper left plot);* *profile of* H_j^k *near the interface at various times (lower left plot);* $\log H_j^k$ *against* $\log(x_c^k - x_j)$ *in the vicinity of the free boundary (upper right plot), and over the whole range* $x_j \in [0, x_c^k)$ *(lower right plot), with a dotted line of gradient* $4/n$ *(from asymptotic theory) in each case.*
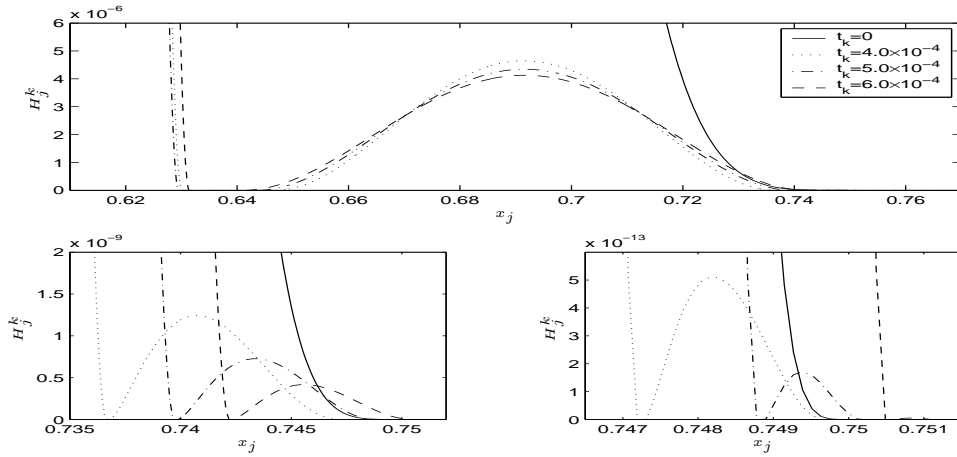

FIG. 4.9. *Numerical results for* $n = 0.75$, $\alpha = 4.5$; *profile of* H_j^k *near the interface at various times (same legend for each plot).*

advancing, with a shorter waiting period in Figure 4.8. In Figures 4.10 and 4.12, x_c^k appears to immediately retreat, wait, and then advance. However, this retreat is over a very short distance, and over a longer timescale the boundary appears to wait; note the different scales on the two plots in the upper left corner of Figure 4.12.

In the lower left corner of Figures 4.6, 4.8, 4.10 and 4.12 we show profiles of H_j^k in the vicinity of the free boundary at various times before the free boundary has begun to advance. In each case the value of H_j^k drops faster further behind the free boundary, leading to the formation of humps near the boundary. In order to demonstrate the existence of more than one such hump, we show profiles of H_j^k on smaller and smaller scales nearer and nearer to the free boundary in Figures 4.7, 4.9, 4.11 and 4.13. Note the different scales on the horizontal and vertical axes of each
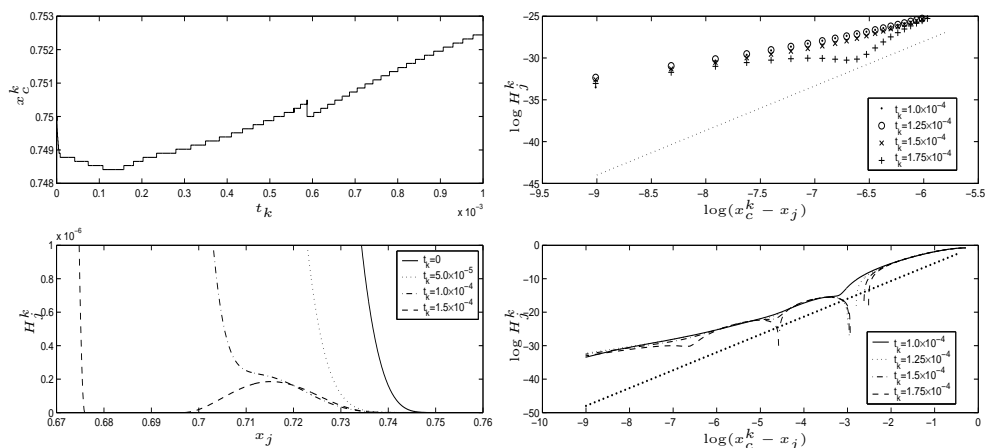
FIG. 4.10. *Numerical results for $n = 0.75$, $\alpha = 4.1$; motion of the numerical free boundary (upper left plot); profile of H_j^k near the interface at various times (lower left plot); $\log H_j^k$ against $\log(x_c^k - x_j)$ in the vicinity of the free boundary (upper right plot), and over the whole range $x_j \in [0, x_c^k)$ (lower right plot), with a dotted line of gradient $4/n$ (from asymptotic theory) in each case.*
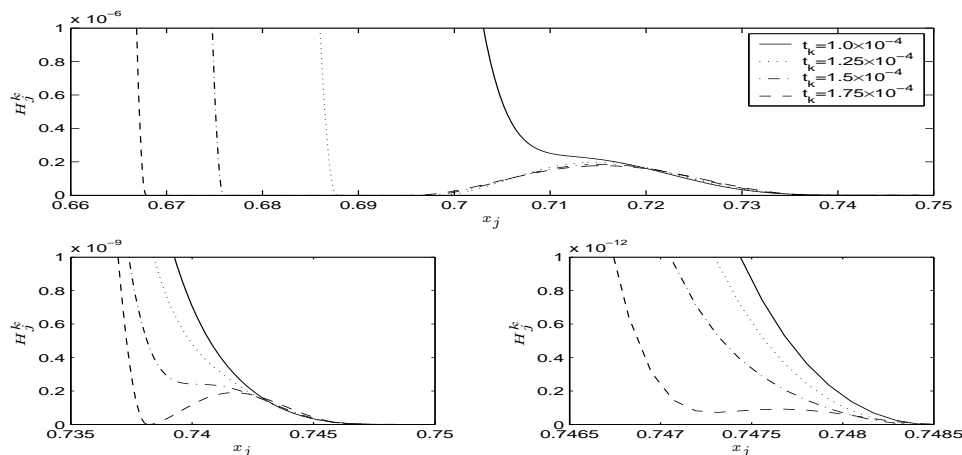

FIG. 4.11. *Numerical results for $n = 0.75$, $\alpha = 4.1$; profile of H_j^k near the interface at various times (same legend for each plot).*

plot in Figures 4.7, 4.9, 4.11 and 4.13

In the upper right corner of Figures 4.6, 4.8, 4.10 and 4.12 we plot $\log H_j^k$ against $\log(x_c^k - x_j)$ in the vicinity of the free boundary at various times before the free boundary has begun to advance. For comparison we also plot a dotted line with slope $4/n$ in each figure. In Figure 4.6, the best fitting least squares line for $t_k = 0$ has a slope of 5.10, rising to 5.26 for $t_k = 2.5 \times 10^{-5}$ and 5.45 for $t_k = 5.0 \times 10^{-5}$. For $t_k = 7.5 \times 10^{-5}$ the log-log plot is no longer very straight. We remark that in this case with $n = 0.75$ and $\alpha = 5.1$, H_j^k is very close to zero quite far behind the free boundary, hence the numerical results are extremely delicate. In Figure 4.8, the log-log plot is not straight immediately in the vicinity of the free boundary for any $t_k > 0$, although it is fairly straight further away from the free boundary. In Figures 4.10 and 4.12, the
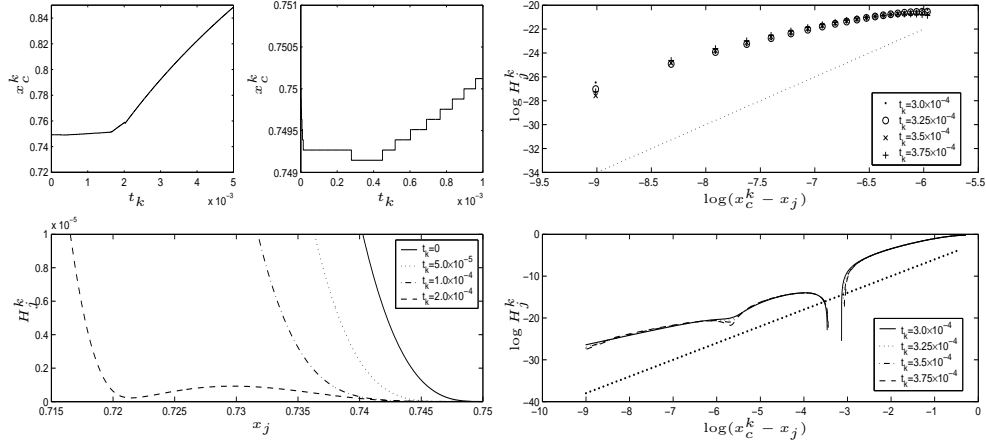
FIG. 4.12. *Numerical results for $n = 1.0$, $\alpha = 3.1$; motion of the numerical free boundary (upper left plots: note the different scales on each figure); profile of H_j^k near the interface at various times (lower left plot); $\log H_j^k$ against $\log(x_c^k - x_j)$ in the vicinity of the free boundary (upper right plot), and over the whole range $x_j \in [0, x_c^k)$ (lower right plot), with a dotted line of gradient $4/n$ (from asymptotic theory) in each case.*
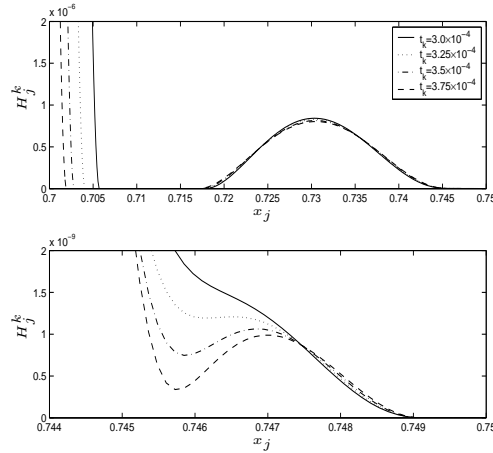

FIG. 4.13. *Numerical results for $n = 1.0$, $\alpha = 3.1$; profile of H_j^k near the interface at various times (same legend for each plot).*

log-log plots are not very straight, and the best fitting least squares lines have slopes significantly lower than $4/n$.

In the lower right corners of Figures 4.6, 4.8, 4.10 and 4.12 we plot $\log H_j^k$ against $\log(x_c^k - x_j)$ over the whole range $x_j \in [0, x_c^k)$ at various times before the free boundary has begun to advance, plotting again a dotted line with slope $4/n$ for comparison. In Figure 4.6, as t_k increases, the log-log plot becomes less and less straight, and for $t_k = 3.0 \times 10^{-3}$ the periodic behaviour of the solution near the interface can clearly be seen. The log-log plots for $t_k = 4.0 \times 10^{-3}$ and $t_k = 5.0 \times 10^{-3}$ are very similar to that for $t_k = 3.0 \times 10^{-3}$ but are not shown here. In Figure 4.8, the formation of humps further and further from the free boundary becomes apparent. For $t_k = 1.0 \times 10^{-4}$,

the slope of the log-log plot away from the free boundary is close to $4/n$. For each of Figures 4.10 and 4.12, as t_k increases the formation of extra humps in the vicinity of the free boundary becomes apparent.

4.6.2. $2 < \alpha < 3/n$. To test the conjecture that the free boundary retreats instantaneously with unbounded velocity, we ran experiments with $n = 1.0$ and $\alpha \in [2.1, 2.9]$. We plot x_c^k against t_k in the left half of Figure 4.14 for $\alpha = 2.2$, 2.4, 2.6 and 2.8. The results support the conjecture. In each case the free boundary retreats, waits, and then advances, although the subsequent advance can only be seen in the figure for $\alpha = 2.2$. The initial velocity of x_c^k appears to decrease as α increases, although as α increases the length of the period for which the free boundary retreats also increases, so that the maximum distance retreated occurs for $\alpha = 2.9$.
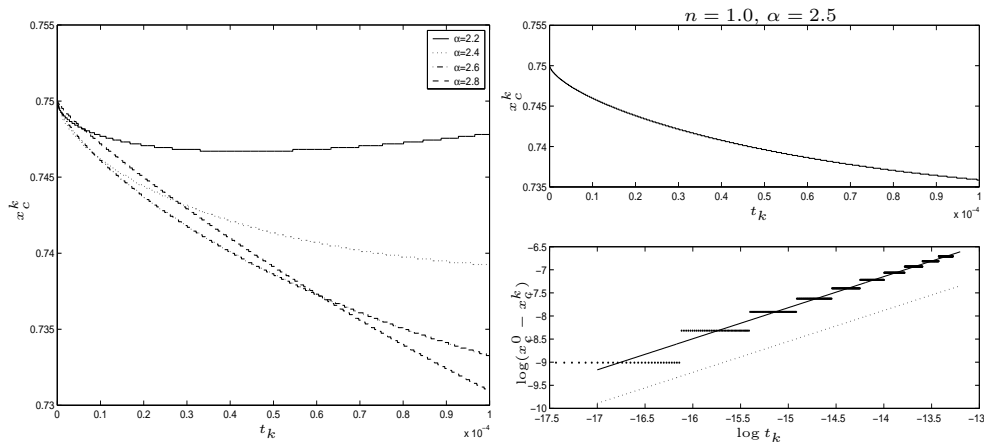

Fig. 4.14. *Numerical results for $n = 1.0$, $2 < \alpha < 3/n$. In the left half of the figure we plot the retreating free boundary for various α. In the right half of the figure we show results for $n = 1.0$, $\alpha = 0.5$: in the upper right section we show the retreating free boundary; in the lower right section we plot $\log t_k$ against $\log(x_c^0 - x_c^k)$ as a discrete set of points, with the solid line following from a least squares fitting and the straight dotted line from asymptotic theory.*

As before we test the hypothesis $x_c^k = x_c^0 - A t_k^\gamma$ for some constants $A > 0$ and γ by plotting $\log(x_c^0 - x_c^k)$ against $\log t_k$. Again, if the hypothesis is correct we expect a straight line with slope γ, and to estimate γ we take a least squares fit over the range for which the log–log plot is approximately straight. In the right half of Figure 4.14 we plot x_c^k against t_k (upper section) and this log–log plot (lower section) for $n = 1.0$ and $\alpha = 2.5$. The log–log plot is approximately straight, and the best fitting least squares line is plotted as a solid line on the same figure. For comparison we also plot a dotted line with slope $(4 - n\alpha)^{-1} = 0.67$. The estimated value of $\gamma = 0.67$ matches this exactly to two decimal places. The expected and estimated values of γ for each value of α tested are shown in Table 4.3. The trend of γ increasing with α is clear, and away from the edges of the parameter regime the estimated value of γ is very close to the expected value.

4.6.3. $\alpha < 2$. To test the conjecture that the free boundary advances instantaneously, with an unbounded velocity, we ran experiments with $n = 1.0$ and $\alpha \in [0.5, 1.9]$. We plot x_c^k against t_k for $\alpha = 0.6$, 0.7, 0.8 and 0.9 (upper left plot), and for $\alpha = 1.5$, 1.6, 1.7 and 1.8 (lower left plot) in Figure 4.15. Note the different time

α	2.1	2.2	2.3	2.4	2.5	2.6	2.7	2.8	2.9
$(4-n\alpha)^{-1}$	0.53	0.56	0.59	0.63	0.67	0.71	0.77	0.83	0.91
γ	0.44	0.53	0.58	0.63	0.67	0.72	0.77	0.81	0.85

TABLE 4.3
Estimated and expected values of γ for $n = 1.0$, various α

scales on the two plots. The results support the conjecture, and the initial velocity of x_c^k decreases as α increases.
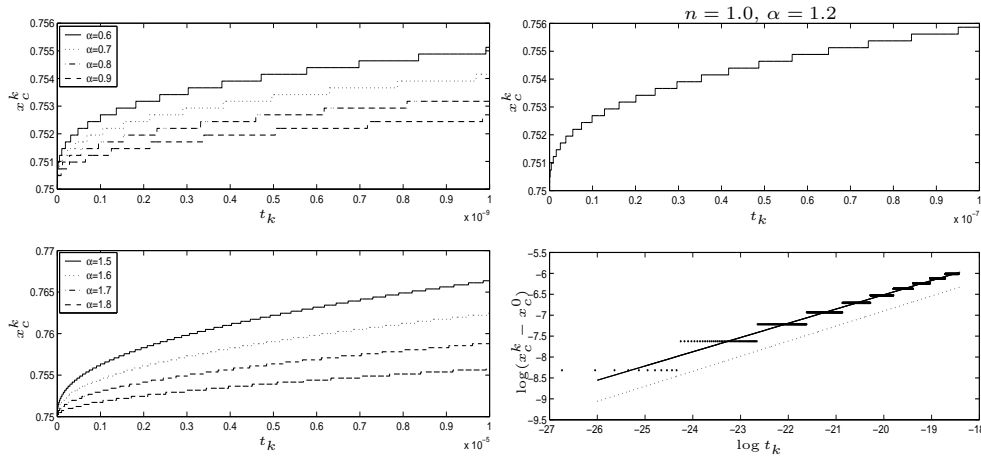

FIG. 4.15. $n = 1.0$, $\alpha < 2$. In the left half of the figure we plot the advancing free boundary for various α (note the different time scales on the two plots). In the right half of the figure we show results for $n = 1.0$, $\alpha = 1.2$: in the upper right section we show the advancing free boundary; in the lower right section we plot $\log t_k$ against $\log(x_c^k - x_c^0)$ as a discrete set of points, with the solid line following from a least squares fitting and the straight dotted line from asymptotic theory.

We again test the hypothesis (4.11), plotting x_c^k against t_k (upper right section of Figure 4.15) and $\log(x_c^k - x_c^0)$ against $\log t_k$ (lower right section of Figure 4.15) for $n = 1.0$ and $\alpha = 1.2$. The log–log plot is approximately straight, and the best fitting least squares line, plotted as a solid line on the same figure, has a slope of 0.34. For comparison we also plot a dotted line with slope $(4-n\alpha)^{-1} = 0.36$ on the same figure. The expected and estimated values of γ are shown in Table 4.4. The trend of γ increasing with α is clear, and for values of α away from the borderline value $\alpha = 2$ the estimated value of γ is very close to the expected value.

α	0.5	0.7	0.9	1.1	1.3	1.5	1.7	1.9
$(4-n\alpha)^{-1}$	0.29	0.30	0.32	0.34	0.37	0.40	0.43	0.48
γ	0.28	0.29	0.31	0.33	0.36	0.40	0.43	0.53

TABLE 4.4
Estimated and expected values of γ for $n = 1.0$, various $\alpha < 2$

5. Conclusions. As we have seen, the thin-film equation (1.1a) exhibits a much broader range of small-time phenomena than its second order analogue, (1.6). Thus, while the behaviour of the former with $2 < n < 3$ corresponds very closely to that of the latter with any $n > 0$, for $n < 2$ equation (1.1a) exhibits a range of α in

which the interface waits but the local profile changes instantaneously from that of the initial data (this combination does not occur for (1.6)), and can exhibit monotonic or oscillatory decay to the local solution (4.14) or limit-cycle behaviour of the form (A.5). Moreover, for $n < 3/2$ fronts can either advance or retreat and our small time classification gives rather precise criteria on the initial data in this regard. The very delicate interlacing of initial profiles leading to immediate expansion or to a finite waiting time, as outlined in §4.4.2, for example, also deserves highlighting.

The high order problem (1.1) is a demanding one from the numerical point of view; this wealth of distinct behaviours occurring over short length and time scales necessitates particularly refined, careful and detailed computational studies if the relevant phenomena are to be captured adequately, and we have sought to implement the required programme of extensive numerical investigations.

A number of generalisations immediately suggest themselves. In higher dimensions, the small-time behaviour of an initially smooth interface will be locally one-dimensional, so most of the conclusions carry over. For $n \geq 3$, the smoothest solutions have fixed interfaces and here waiting-time phenomena relate (for $3 \leq n < 4$) to a delay in the contact angle becoming finite; we shall not elaborate on such matters here, noting only that the approaches we have described above apply equally well in such contexts. As a final instance, we note that for $n < 3$ a finite contact angle condition can be imposed in place of the second of (1.1c) and a similar investigation performed; again, we shall not report the results of such a study here.

REFERENCES

[1] S. ANGENENT, *Solutions of the one-dimensional porous-medium equation are determined by their free boundary*, J. London Math. Soc, 42 (1990), pp. 339–353.

[2] J. W. BARRETT, J. F. BLOWEY, AND H. GARCKE, *Finite element approximation of a fourth order nonlinear degenerate parabolic equation*, Numer. Math., 80 (1998), pp. 525–556.

[3] J. W. BARRETT AND S. LANGDON, *A multigrid method for a fourth order elliptic system.* (in preparation).

[4] J. BECKER AND G. GRÜN, *The thin-film equation: recent advances and some new perspectives*, J. Phys. Condens. Matter, 17 (2005), pp. S291–S307.

[5] E. BERETTA, M. BERTSCH, AND R. DAL PASSO, *Nonnegative solutions of a 4th-order nonlinear degenerate parabolic equation*, Arch. Ration. Mech. Anal., 129 (1995), pp. 175–200.

[6] F. BERNIS, *Viscous flows, fourth order nonlinear degenerate parabolic equations and singular elliptic problems*, in Free boundary problems: theory and applications, A. L. J. I. Diaz, M. A. Herrero and J. L. Vazquez, eds., vol. 323 of Pitman Research Notes in Mathematics, Longman, Harlow, 1995, pp. 40–56.

[7] ———, *Finite speed of propagation and continuity of the interface for thin viscous flows*, Adv. in Diff. Equations, 1 (1996), pp. 337–368.

[8] ———, *Finite speed of propagation for thin viscous flows when $2 \leq n < 3$*, C. R. Acad. Sci. Paris; Sér. I Math., 322 (1996), pp. 1169–1174.

[9] F. BERNIS AND A. FRIEDMAN, *Higher order nonlinear degenerate parabolic equations*, J. Differential Equations, 83 (1990), pp. 179–206.

[10] A. L. BERTOZZI, *Symmetric singularity formation in lubrication-type equations for interface motion*, SIAM J. Appl. Math., 56 (1996), pp. 681–714.

[11] ———, *The mathematics of moving contact lines in thin liquid films*, Notices of the AMS, 45 (1998), pp. 689–697.

[12] A. L. BERTOZZI, M. P. BRENNER, T. F. DUPONT, AND L. P. KADANOFF, *Singularities and similarities in interface flows*, in Trends and Perspectives in Applied Mathematics, L. Sirovich, ed., vol. 100 of Appl. Math. Sci., Springer-Verlag, New York, 1994, pp. 155–209.

[13] A. L. BERTOZZI, G. GRÜN, AND T. P. WITELSKI, *Dewetting films: bifurcations and concentrations*, Nonlinearity, 14 (2001), pp. 1569–1592.

[14] A. L. BERTOZZI AND M. PUGH, *The lubrication approximation for thin viscous films: regularity and long time behaviour of weak solutions.*, Comm. Pure Appl. Math., 49 (1996), pp. 85–123.

[15] J. F. BLOWEY, J. R. KING, AND S. LANGDON, *Small- and waiting-time behaviour of the thin-film equation.* Brunel University Department of Mathematical Sciences Technical Report TR/03/03, 2003.

[16] R. DAL PASSO, H. GARCKE, AND G. GRÜN, *On a fourth order degenerate parabolic equation: global entropy estimates and qualitative behaviour of solutions*, SIAM J. Math. Anal., 29 (1998), pp. 321–342.

[17] R. DAL PASSO, L. GIACOMELLI, AND G. GRÜN, *A waiting time phenomenon for thin film equations*, Ann. Scuola Norm. Sup. Pisa Cl. Sci., 30 (2001), pp. 437–463.

[18] E. B. DUSSAN AND S. H. DAVIS, *On the motion of a fluid-fluid interface along solid surface*, J. Fluid Mech., 65 (1974), pp. 71–95.

[19] H. P. GREENSPAN, *On the motion of a small viscous droplet that wets a surface*, J. Fluid Mech., 84 (1978), pp. 125–143.

[20] G. GRÜN, *Droplet spreading under weak slippage: the waiting time phenomenon*, Ann. Inst. H. Poincaré Anal. Non Linéaire, 21 (2004), pp. 255–269.

[21] G. GRÜN AND M. RUMPF, *Nonnegativity preserving convergent schemes for the thin film equation*, Numer. Math., 87 (2000), pp. 113–152.

[22] R. E. GRUNDY, *Local similarity solutions for the initial-value problem in non-linear diffusion*, IMA J. Appl. Math., 30 (1983), pp. 209–214.

[23] L. M. HOCKING, *Sliding and spreading of thin two-dimensional drops*, Quart. J. Mech. Appl. Math., 34 (1981), pp. 37–55.

[24] E. HUH AND L. E. SCRIVEN, *Hydrodynamic model of steady movement of a solid / liquid / fluid contact line*, J. Colloid Interface Sci., 35 (1971), pp. 85–101.

[25] J. R. KING, *Exact polynomial solutions to some nonlinear diffusion equations*, Phys. D, 64 (1993), pp. 35–65.

[26] ———, *Development of singularities in some moving boundary problems*, European J. Appl. Math., 6 (1995), pp. 491–507.

[27] J. R. KING AND M. BOWEN, *Moving boundary problems and non-uniqueness for the thin film equation*, European J. Appl. Math., 12 (2001), pp. 321–356.

[28] A. A. LACEY, *Initial motion of the free-boundary for a non-linear diffusion equation*, IMA J. Appl. Math., 31 (1983), pp. 113–119.

[29] A. A. LACEY, J. R. OCKENDON, AND A. B. TAYLER, *Waiting-time solutions of a nonlinear diffusion equation*, SIAM J. Appl. Math., 42 (1982), pp. 1252–1264.

[30] T. G. MYERS, *Thin films with high surface tension*, SIAM Rev., 40 (1998), pp. 441–462.

Appendix A. Applicability of the local solution (4.4). In this appendix we use boundary condition counting arguments to assess the applicability of (4.4) as a local solution to (4.2) for $0 < n < 2$. Writing

$$f \sim \left(\frac{n^3}{8(4-n)(2-n)(n+4)}(-\eta)^4 \right)^{\frac{1}{n}} + F \tag{A.1}$$

and linearising yields

$$\frac{1}{4-n\alpha}(\alpha F - \eta F_\eta) = -\frac{n^3}{8(4-n)(2-n)(n+4)}\frac{\mathrm{d}}{\mathrm{d}\eta}\left(\eta^4 \frac{\mathrm{d}^3 F}{\mathrm{d}\eta^3} \right) - \frac{n}{n+4}\frac{\mathrm{d}}{\mathrm{d}\eta}\left(\eta F \right),$$

with solutions

$$F = K(-\eta)^p \tag{A.2}$$

where the possible p are the roots of the quartic

$$\frac{n^3 p(p-1)(p-2)(p+1)}{8(4-n)(2-n)(n+4)} + \frac{n(p+1)}{n+4} + \frac{\alpha-p}{4-n\alpha} = 0. \tag{A.3}$$

The expansion of (A.1) with F given by (A.2) is self-consistent if $\mathrm{Re}(p) > 4/n$, so the relations between α and n such that two roots of (A.3) have $\mathrm{Re}(p) = 4/n$ are crucial; these relations can be shown to be

$$\alpha_1(n) = \frac{\alpha_{-b} + \alpha_\Delta}{\alpha_d}, \quad \alpha_2(n) = \frac{\alpha_{-b} - \alpha_\Delta}{\alpha_d},$$

where

$$\alpha_d = 2\left(n^2 - n - 8\right)\left(7\,n^3 - 84\,n^2 + 400\,n - 640\right)n,$$
$$\alpha_{-b} = 47n^5 - 674n^4 + 3384n^3 - 3520n^2 - 17408n + 36864,$$
$$\alpha_\Delta = (n+4)(2-n)(8-n)\sqrt{9216 - 5632n + 896n^2 + 112n^3 - 31n^4},$$

so that

$$\alpha_1 \sim 2 + \frac{11}{10}\left(2-n\right) + O\!\left((2-n)^2\right) \text{ as } n \to 2^-, \quad \alpha_1 \sim \frac{3}{n} + \frac{5}{24} + O\left(n\right) \text{ as } n \to 0^+,$$
$$\alpha_2 \sim 2 + \frac{31}{22}\left(2-n\right)^2 + O\!\left((2-n)^3\right) \text{ as } n \to 2^-, \quad \alpha_2 \sim \frac{21}{5n} - \frac{1}{120} + O(n) \text{ as } n \to 0^+.$$

It is also instructive to note the curves in (α, n) space on which roots of (A.3) become complex, namely the repeated roots case in which (A.3) and

$$\frac{\mathrm{d}}{\mathrm{d}p}\left[\frac{n^3 p(p-1)(p-2)(p+1)}{8(4-n)(2-n)(n+4)} + \frac{n(p+1)}{n+4} + \frac{\alpha - p}{4 - n\alpha}\right] = 0 \qquad (A.4)$$

are satisfied simultaneously. The various curves relevant to our discussion are shown in Figure A.1. In particular we define $\alpha_5 = \alpha_5(n)$ to be the repeated root case (v_b) shown in Figure A.1.
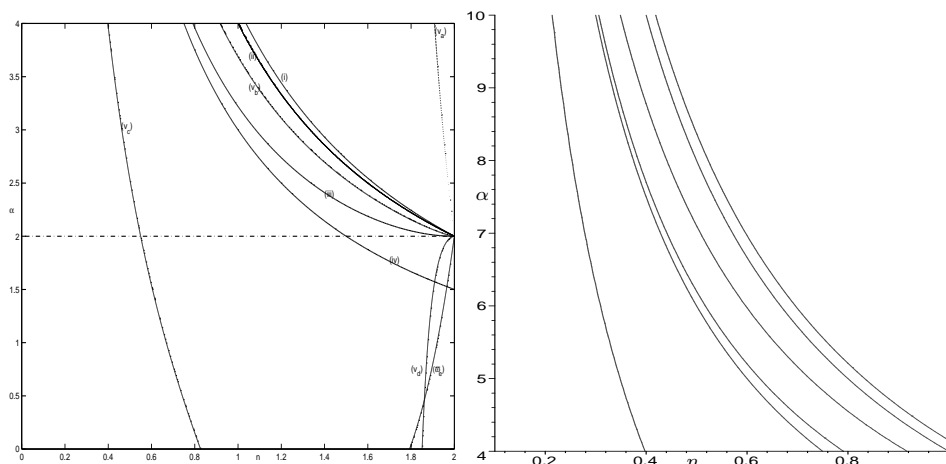

FIG. A.1. (α, n) space; (i) $\alpha = \alpha_1$, (ii) $\alpha = 4/n$, (iii) $\alpha = \alpha_2$, (iv) $\alpha = 3/n$, (v) the solutions to (A.3) and (A.4). To the right of (v_a) and of the right most of (v_d) and (v_e) there are four real roots; between (v_a) and (v_b), between (v_d) and (v_e) and to the left of (v_c) there are two real and two complex roots; between (v_c), (v_b) and the left most of (v_d) and (v_e) there are four complex roots. Three of the roots become unbounded as (ii) is approached, with the fourth having $p \sim 4/n$. Above (i) and below (iii), none of the roots have $\operatorname{Re}(p) > 4/n$; between (iii) and (v_b), two of the four complex roots have $\operatorname{Re}(p) > 4/n$ and the other two $\operatorname{Re}(p) < 4/n$; between (v_b) and (ii) both real roots satisfy $p > 4/n$ and both complex ones $\operatorname{Re}(p) < 4/n$; between (ii) and (i) the real roots have $p < 4/n$ and the complex ones $\operatorname{Re}(p) > 4/n$.

In $\alpha_2 < \alpha < \frac{4}{n}$, two roots of (A.3) have $\operatorname{Re}(p) > \frac{4}{n}$ and the local expansion (A.1) is correctly specified (the two degrees of freedom being the K's in (A.2) corresponding to those two roots). As α drops below α_2 we anticipate that a Hopf bifurcation occurs

in (4.2)–(4.3a,b) with the local behaviour as $\eta \to 0^-$ taking for $\alpha > \max(2, 3/n)$ the "limit-cycle" form

$$f \sim (-\eta)^{\frac{4}{n}} \Omega(-\ln(-\eta)) \tag{A.5}$$

where $\Omega(\xi)$ is periodic of period P, say, in ξ. Since on $\alpha = \alpha_2$

$$\text{Im}(p) = \pm \frac{1}{\sqrt{2n}} \sqrt{96 - 24n - n^2 - \sqrt{9216 - 5632n + 896n^2 + 112n^3 - 31n^4}},$$

we anticipate that

$$P \sim \frac{2\sqrt{2}\pi n}{\sqrt{96 - 24n - n^2 - \sqrt{9216 - 5632n + 896n^2 + 112n^3 - 31n^4}}} \quad \text{as } \alpha \to \alpha_2^-.$$

Note that P will depend on α and n but, in view of the scaling properties of (4.2)–(4.3a,b), not on A_0. For $\alpha_5 < \alpha < \frac{4}{n}$, the decay to (4.4) is non-oscillatory while for $\alpha_2 < \alpha < \alpha_5$ damped oscillations occur.

Appendix B. $3/2 < n < 2$, $\alpha \to 2$. We are concerned here with the behaviour of (4.2)-(4.3a,b) for α close to two. Writing $\alpha = 2 + \epsilon$, $0 < |\epsilon| \ll 1$, we have for $\eta = O(1)$ that

$$f \sim A_0(-\eta)^2 + \epsilon f_1(\eta) \tag{B.1}$$

with

$$\frac{1}{2(2-n)} \left(2f_1 - \eta \frac{df_1}{d\eta} + A_0(-\eta)^2 \right) = -A_0^n \frac{d}{d\eta} \left((-\eta)^{2n} \frac{d^3 f_1}{d\eta^3} \right), \tag{B.2a}$$

$$\text{as } \eta \to -\infty \quad f_1 \sim A_0(-\eta)^2 \ln(-\eta) - 2(2n-1)A_0^{n+1}(-\eta)^{2(n-1)}, \tag{B.2b}$$

$$\text{as } \eta \to 0^- \quad f_1 = (-\eta)^{2n} \frac{d^3 f_1}{d\eta^3} = 0. \tag{B.2c}$$

It follows from (B.2a–c) that

$$f_1 \sim -\mu(n) A_0^{\frac{4-n}{2(2-n)}} (-\eta) \quad \text{as } \eta \to 0^+; \tag{B.3}$$

we believe the constant μ, which is determined as part of the solution to (B.2a–c), to be positive; the dependence on A_0 in (B.3) follows from rescaling f_1 by $A_0^{2/(2-n)}$ and η by $A_0^{n/(2(2-n))}$ in (B.2a–c).

The expansion (B.1) breaks down for small η with inner scalings $\eta = |\epsilon|\xi$, $f = |\epsilon|^2 g(\xi)$ and $\frac{d}{d\xi} \left(g_0^n \frac{d^3 g_0}{d\xi^3} \right) = 0$. For $\epsilon < 0$ we thus have

$$g_0 = A_0(\xi_0 - \xi)^2, \quad \xi_0 = \frac{1}{2}\mu A_0^{\frac{n}{2(2-n)}}, \tag{B.4}$$

with $\eta_0 \sim |\epsilon|\xi_0$ and with inner-inner scalings $\eta = \eta_0 + |\epsilon|^{1/(2n-3)}\zeta$, $f = |\epsilon|^{2/(2n-3)}h(\zeta)$, whereby

$$\frac{1}{2(2-n)}\xi_0 = h_0^{n-1} \frac{d^3 h_0}{d\zeta^3},$$

$$\text{as } \zeta \to -\infty \quad h_0 \sim A_0(-\zeta)^2,$$

$$\text{as } \zeta \to 0^- \quad h_0 \sim \left(\frac{n^3 \xi_0}{6(3-n)(2n-3)(2-n)} (-\zeta)^3 \right)^{\frac{1}{n}},$$

producing the desired local behaviour (1.2). However, for $\epsilon > 0$ the expression (B.4) is replaced by

$$g_0 = A_0(-\xi_0 - \xi)^2, \quad \xi_0 = \frac{1}{2}\mu A_0^{\frac{n}{2(2-n)}}, \tag{B.5}$$

and (recalling that the interface cannot contract for $n > 3/2$) the inner-inner scalings read $\xi = -\xi_c(\epsilon) + \epsilon^{2(2-n)/(2n-3)}\zeta$, $g = \epsilon^{4(2-n)/(2n-3)}h(\zeta)$, where $\xi_c(0) = \xi_0$ and

$$-\frac{1}{2(2-n)}\xi_0(h_0 - H_\infty) = h_0^n \frac{\mathrm{d}^3 h_0}{\mathrm{d}\zeta^3}, \tag{B.6a}$$

$$\text{as } \zeta \to -\infty \quad h_0 \sim A_0(-\zeta)^2, \tag{B.6b}$$

$$\text{as } \zeta \to \infty \quad h_0 \to H_\infty, \tag{B.6c}$$

which determines both h_0 (up to translations in ζ) and H_∞, the decay of h_0 to H_∞ being non-oscillatory. In $-\xi_0 < \xi < 0$ we then have

$$h \sim H_\infty \frac{(-\xi)^2}{\xi_0^2}, \tag{B.7}$$

the left-hand side of (4.2) dominating. The scaling properties of (B.6a–c) show that h_0 and H_∞ scale with $A_0^{2/(2-n)}$ and ζ with $A_0^{n/(2(2-n))}$, so we may rewrite (B.7) as

$$h \sim \nu(n)A_0(-\xi)^2. \tag{B.8}$$

Now setting

$$f = \nu^{\frac{2}{2-n}}\epsilon^{\frac{8}{2n-3}}\widehat{f}, \quad \eta = \nu^{\frac{n}{2(2-n)}}\epsilon^{\frac{2n}{2n-3}}\widehat{\eta}, \tag{B.9}$$

we have that

$$\widehat{f} \sim A_0(-\widehat{\eta})^2 + \epsilon f_1(\widehat{\eta}),$$

where f_1 satisfies (B.2a–c) with η replaced by $\widehat{\eta}$, implying that the above structure repeats itself on a sequence of finer and finer scales, consistent with the limit cycle behaviour referred to in Appendix A. Thus if we denote the variables in the mth member of the sequence by $f^{(m)}$, $\eta^{(m)}$ with $f^{(0)} = f$ and $\eta^{(0)} = \eta$ we have from (B.9) that

$$f^{(m)} \sim \nu^{\frac{2}{2-n}}\epsilon^{\frac{8}{2n-3}}f^{(m-1)}, \quad \eta^{(m)} \sim \nu^{\frac{n}{2(2-n)}}\epsilon^{\frac{2n}{2n-3}}\eta^{(m-1)},$$

implying that

$$f^{(m)}(\eta) \sim \nu^{\frac{2m}{2-n}}\epsilon^{\frac{8m}{2n-3}}f\left(\frac{\eta}{\nu^{\frac{mn}{2(2-n)}}\epsilon^{\frac{2mn}{2n-3}}}\right),$$

where leading order expressions for f on the right-hand side are given through a single cycle of the oscillation by (B.1), (B.5), (B.6a–c), (B.8). This is consistent with (A.5) with

$$P \sim \frac{2n}{2n-3}\ln\left(\frac{1}{\epsilon}\right) - \frac{n}{2(2-n)}\ln\nu$$

being large; note that the region described by (B.6a–c) is particularly significant because it leads to the $(-\eta)^{4/n}$ type decay in (A.5) despite the solution behaving quadratically in other regions.